thymectomized-NFS/sld mice than in the control mice that did not undergo thymectomy.

- Five genes, *mpt1, Laptm5, UCP2 Gnai2* and *IL16*, have not been identified previously as SS-related genes.
- Human *Grap* and *Laptm5* protein antigens were expressed on certain infiltrated lymphocytes and on ductal cells in the salivary glands from patients with SS, but very weakly in control subjects.

References

[1] Talal N, Sokoloff L, Barth WF. Extrasalivary lymphoid abnormalities in Sjögren's syndrome reticulum cell sarcoma, "pseudolymphoma", macroglobulinemia. Am J Med 1967; 43:50–65.

[2] Hoffman RW, Alspaugh MA, Waggle KS, Durham JB, Walker SE. Sjögren's syndrome in MRL/lpr and MRL/n mice. Arthritis Rheum 1984;27:157–65.

[3] Moutsopoulous HM, Fauci AS. Immunoregulation in Sjögren's syndrome: influence of serum factors on T-cell subpopulations. J Clin Invest 1980;65:519–28.

[4] Fox RI. Clinical feature, pathogenesis, and treatment of Sjögren's syndrome. Curr Opin Rheumatol 1996;8:438–45.

[5] Izui S, Kelley VE, Masuda K, Yoshida H, Roths JB, Murphy ED. Induction of various autoantibodies by mutant gene *lpr* in several strains of mice. J Immunol 1984;133: 227–33.

[6] Watanabe-Fukunaga R, Brannan CI, Copeland NG, Jenkins NA, Nagata S. Lymphoproliferation disorder in mice explained by defects in Fas antigen that mediates apoptosis. Nature 1992;356:314–7.

[7] Hayashi Y, Haneji N, Hamano H. Pathogenesis of Sjögren's syndrome-like autoimmune lesions in MRL/lpr mice. Pathol Int 1994;44:559–68.

[8] Jabs DA, Lee B, Whittum-Hudson J, Prendergast RA. The role of Fas–Fas ligand-mediated apoptosis in autoimmune lacrimal gland disease in MRL/MpJ mice. Invest Ophthalmol Vis Sci 2001;42:399–401.

[9] Cohen PL, Eisenberg RA. *Lpr* and *gld* single gene models of systemic autoimmunity and lymphoproliferative disease. Annu Rev Immunol 1991;9:243–69.

[10] Nakatsuru S, Terada M, Nishihara M, Kamogawa J, Miyazaki T, Qu WM, et al. Genetic dissection of the complex pathological manifestations of collagen disease in MRL/lpr mice. Pathol Int 1999;49:974–82.

[11] Haneji N, Hamano H, Yanagi K, Hayashi Y. A new animal model for primary Sjögren's syndrome in NFS/sld mutant mice. J Immunol 1994;153:2769–77.

[12] Hayashi Y, Haneji N, Hamano H, Yanagi K, Takahashi M, Ishimaru N. Effector mechanism of experimental autoimmune sialoadenitis in the mouse model for primary Sjögren's syndrome. Cell Immunol 1996;171:217–25.

[13] Liang P, Pardee AB. Differential display of eukaryotic messenger RNA by means of the polymerase chain reaction. Science 1992;257:967–71.

[14] Diatchenko L, Lau YF, Campbell AP, Chenchik A, Moqadam F, Huang B, et al. Suppression subtractive hybridization: a method for generating differentially regulated or tissue-specific cDNA probes and libraries. Proc Natl Acad Sci USA 1996;93:6025–30.

[15] Schena M, Shalon D, Davis RW, Brown PO. Quantitative monitoring of gene expression patterns with a complementary DNA microarray. Science 1995;270:467–70.

[16] Velculescu VE, Zhang L, Vogelstein B, Kinzler KW. Serial analysis of gene expression. Science 1995;270:484–7.

[17] Brown PO, Botstein D. Exploring the new world of the genome with DNA microarrays. Nat Genet 1999;21:33–7.

[18] Yoshikawa T, Nagasugi Y, Azuma T, Kato M, Sugano S, Hashimoto K, et al. Isolation of novel mouse genes differentially expressed in brain using cDNA microarray. Biochem Biophys Res Commun 2000;275:532–7.

[19] Alizadeh AA, Eisen MB, Davis RE, Ma C, Lossos IS, Rosenwald A, et al. Distinct types of diffuse large B-cell lymphoma identified by gene expression profiling. Nature 2000;403: 503–11.

[20] Luthi-Carter R, Strand A, Peters NL, Solano SM, Hollingsworth ZR, Menon AS, et al. Decreased expression of striatal signaling genes in a mouse model of Huntington's disease. Hum Mol Genet 2000;9:1259–71.

[21] Stanton LW, Garrard LJ, Damm D, Garrick BL, Lam A, Kapoun AM, et al. Altered patterns of gene expression in response to myocardial infarction. Circ Res 2000;86: 939–45.

[22] van Blokland SC, van Helden-Meeuwsen CG, Wierenga-Wolf AF, Drexhage HA, Hooijkaas H, van de Merwe JP, et al. Two different types of sialoadenitis in the NOD- and MRL/lpr mouse models for Sjögren's syndrome: a differential role for dendritic cells in the initiation of sialoadenitis? Lab Invest 2000;80:575–85.

[23] Azuma T, Takei M, Yoshikawa T, Nagasugi Y, Kato M, Shiraiwa H, et al. Identification of candidate genes for Sjogren's syndrome using MRL/lpr mouse model of Sjögren's syndrome and cDNA microarray analysis. Immunol Lett 2002;81:171–6.

[24] Robinson CP, Yamachika S, Alford CE, Cooper C, Pichardo EL, Shah N, et al. Elevated levels of cysteine protease activity in saliva and salivary glands of the nonobese diabetic (NOD) mouse model for Sjogren syndrome. Proc Natl Acad Sci USA 1997;94:5767–71.

[25] Dumont FJ. Stimulation of murine T cells via the Ly-6C antigen: lack of proliferative response in aberrant T cells from lpr/lpr and gld/gld mice despite high Ly-6C antigen expression. J Immunol 1987;138:4106–13.

[26] Andre-Schwartz J, Datta SK, Shoenfeld Y, Isenberg DA, Stollar BD, Schwartz RS. Binding of cytoskeletal proteins by monoclonal anti-DNA lupus autoantibodies. Clin Immunol Immunopathol 1984;31:261–71.

[27] Kjorell U, Ostberg Y. Distribution of intermediate filaments and actin microfilaments in parotid autoimmune sialoadenitis of Sjögren syndrome. Histopathology 1984;8:991–1011.

[28] Takahashi M, Mimura Y, Hayashi Y. Role of the ICAM-1/LFA-1 pathway during the development of autoimmune dacryoadenitis in an animal model for Sjögren's syndrome. Pathobiology 1996;64:269–74.
[29] Steinfeld S, Maho A, Chaboteaux C, Daelemans P, Pochet R, Appelboom T, et al. Prolactin up-regulates cathepsin B and D expression in minor salivary glands of patients with Sjögren's syndrome. Lab Invest 2000;80:1711–20.
[30] Fujihara T, Fujita H, Tsubota K, Saito K, Tsuzaka K, Abe T, et al. Preferential localization of CD8+ (E)7+ T cells around acinar epithelial cells with apoptosis in patients with Sjögren's syndrome. J Immunol 1999;163:2226–35.
[31] Liu SK, Berry DM, McGlade CJ. The role of Gads in hematopoietic cell signaling. Oncogene 2001;20:6284–90.
[32] Shiraiwa H, Takei M, Yoshikawa T, Azuma T, Kato M, Mitamura K, et al. Detection of Grb-2-related adaptor protein gene (GRAP) and peptide molecule in salivary glands of MRL/lpr mice and patients with Sjögren's syndrome. J Int Med Res 2004;32:284–91.
[33] Aikawa Y, Hara H, Watanabe T. Molecular cloning and characterization of mammalian homologues of the drosophila retinal degeneration Bgene. Biochem Biophys Res Commun 1997;236:559–64.
[34] Cockcroft S. Phosphatidylinositol transfer proteins: a requirement in signal transduction and vesicle traffic. Bioessays 1998;20:423–32.
[35] Tomita-Yamaguchi M, Santoro TJ. Constitutive turnover of inositol-containing phospholipids in B220+ T cells from autoimmune-prone MRL-lpr/lpr mice. J Immunol 1990;144:3946–52.
[36] Adra CN, Zhu S, Ko JL, Guillemot JC, Cuervo AM, Kobayashi H, et al. *LAPTM5*: A novel lysosomal-associated multispanning membrane protein preferentially expressed in hematopoietic cells. Genomics 1996;35:328–37.
[37] Arsenijevic D, Onuma H, Pecqueur C, Raimbault S, Manning BS, Miroux B, et al. Disruption of the uncoupling protein-2 gene in mice reveals a role in immunity and reactive oxygen species production. Nat Genet 2000;26:435–9.
[38] Masaki T, Yoshimatsu H, Chiba S, Hidaka S, Tajima D, Kakuma T, et al. Tumor necrosis factor—regulates in vivo expression of the rat UCP family differentially. Biochim Biophys Acta 1999;1436:585–92.
[39] Chan OT, Madaio MP, Shlomchik MJ. The central and multiple roles of B cells in lupus pathogenesis. Immunol Rev 1999;169:107–21.

Endometriosis and systemic lupus erythematosus: a comparative evaluation of clinical manifestations and serological autoimmune phenomena.

Due to evidences suggesting association between endometriosis (EM) and systemic lupus erythematosus (SLE), Pasoto SG. et al. (Am J Reprod Immunol 2005;53:85–93), have performed a comparative evaluation of clinical and humoral immunologic abnormalities in both diseases. Forty-five women with histologically confirmed pelvic EM, 21 healthy-women and 15 female SLE-patients without surgically confirmed EM were prospectively evaluated. None of the EM-patients fulfilled criteria for SLE. However, EM-patients presented higher frequencies of arthralgia (62%) and generalized myalgia (18%) compared to that of normal-controls (24%, $p = 0.04$) but comparable with SLE-patients. Antinuclear antibodies (ANA) were detected in 18% of EM-patients, as compared with healthy-women ($p = 0.01$). Anti-Ro and anticardiolipin antibodies were more often in SLE (40%, 33%) than in EM-patients (2%, $p < 0.001$ and 9% $p = 0.04$). Elevated immune-complexes and low total complement were also more frequent in SLE patients. The data indicate differences of ANA antigenic specificity and complement consumption between EM and SLE. The high prevalence of generalized musculoskeletal complaints in EM justifies a multidisciplinary approach.

Two cases of antinuclear antibody negative lupus showing increased proportion of B cells lacking RP105.

B cells lacking RP105 molecule, a member of the Toll-like receptor family, were increased in the peripheral blood of 2 patients with antinuclear antibody (ANA) negative systemic lupus erythematosus (SLE). The increased proportion of RP105-lacking B cells was associated with disease activity in patients with ANA-negative SLE. Koarada S. et al (J Rheumatol 2005; 32:562-4) suggested that when there are no significant serological markers for SLE, analyses of expression of RP105 may be helpful in evaluation of activity in ANA-negative SLE. Thus they describe a new approach, using phenotyping of B cells, to evaluate activity of ANA-negative SLE.

nature genetics

Mutations in the gene encoding fibroblast growth factor 10 are associated with aplasia of lacrimal and salivary glands

Miriam Entesarian[1], Hans Matsson[1], Joakim Klar[1], Birgitta Bergendal[2], Lena Olson[3], Rieko Arakaki[4], Yoshio Hayashi[4], Hideyo Ohuchi[5], Babak Falahat[6], Anne Isine Bolstad[7], Roland Jonsson[8], Marie Wahren-Herlenius[9] & Niklas Dahl[1]

Autosomal dominant aplasia of lacrimal and salivary glands (ALSG; OMIM 180920 and OMIM 103420) is a rare condition characterized by irritable eyes and dryness of the mouth. We mapped ALSG to 5p13.2–5q13.1, which coincides with the gene fibroblast growth factor 10 (*FGF10*). In two extended pedigrees, we identified heterozygous mutations in *FGF10* in all individuals with ALSG. *Fgf10*$^{+/-}$ mice have a phenotype similar to ALSG, providing a model for this disorder. We suggest that haploinsufficiency for FGF10 during a crucial stage of development results in ALSG.

ALSG has variable expressivity, and affected individuals may have aplasia or hypoplasia of the lacrimal, parotid, submandibular and sublingual glands and absence of the lacrimal puncta[1]. The disorder is characterized by irritable eyes, recurrent eye infections, epiphora (constant tearing) and xerostomia (dryness of the mouth), which increases the risk of dental erosion, dental caries, periodontal disease and oral infections[2]. Individuals affected with ALSG are sometimes misdiagnosed with the more prevalent disorder Sjögren syndrome, an autoimmune disorder characterized by keratoconjunctivitis sicca and xerostomia[3]. Both sporadic and familial cases of ALSG have been described[2,4,5]. We recently identified two extended families of Swedish origin with ALSG (**Fig. 1a**). The phenotypes of the affected individuals are summarized in **Supplementary Table 1** online. In total, 16 individuals from both families were diagnosed with ALSG (**Supplementary Methods** online). We investigated the lacrimal and major salivary glands by magnetic resonance imaging (**Supplementary Fig. 1** online), which showed aplasia or hypoplasia of several major salivary glands in all affected individuals and absent or hypoplastic lacrimal glands in 13 of 14 affected individuals. We observed absence of one or several lacrimal puncta in 13 of 14 affected individuals. We observed no other abnormalities, and the affected individuals had normal lifespans.

Inheritance of ALSG in both families is autosomal dominant, and the segregation pattern suggested full penetrance. A genome-wide screen with 400 polymorphic microsatellite markers showed linkage of ALSG to 5p13.2–5q13.1 flanked by microsatellite markers *D5S395* and *D5S2046* (**Fig. 1a**). We obtained a maximum cumulative lod score of 5.72 ($\theta = 0$) at the marker locus *D5S398* for both families (**Supplementary Table 2** online). The gene fibroblast growth factor 10 (*FGF10*) is located in the linked region[6]. Mouse FGF10, which is 93% identical to human FGF10, is crucial for the development of several organs, including lacrimal and salivary glands[7–9]. *Fgf10*$^{-/-}$ mice die shortly after birth[9,10]. No abnormalities have been described in *Fgf10*$^{+/-}$ mice.

We considered *FGF10* as a candidate gene for ALSG. Sequence analysis of the three exons of *FGF10* in samples from family 1 showed no alterations compared with sequences in the National Center for Biotechnology Information database. To identify deletions, we genotyped the family members for SNPs and microsatellite markers in *FGF10*. The affected members of family 1 were hemizygous with respect to two dinucleotide repeats (TA53 and CA17) and three SNPs (rs10060548, rs6881797 and rs2290070; **Fig. 1b,c**). After genotyping, we characterized the deletion breakpoint by long-range PCR and sequencing across the breakpoint (**Supplementary Fig. 2** online). We determined the size of the deletion to be 53 kb, including exons 2 and 3, without the involvement of any flanking genes (**Fig. 1b**). In family 2, DNA sequence analysis of *FGF10* identified a heterozygous stop mutation in exon 3 (R193X; 577C→T) resulting in a predicted truncated protein in the four affected members (**Fig. 1d**).

We then reexamined *Fgf10*$^{+/-}$ mice, which were previously described as apparently normal[8,10]. We dissected adult mice and carried out a macroscopical and histological examination of the lacrimal and salivary gland apparatuses. *Fgf10*$^{+/-}$ mice had aplasia of lacrimal glands and hypoplasia of salivary glands (**Fig. 2**). These findings are consistent with the phenotype of individuals with ALSG. Other internal organs, including lung, liver, spleen, heart, stomach, thyroid, pancreas, intestines and ovaries, were macroscopically normal in *Fgf10*$^{+/-}$ mice.

To clarify whether *FGF10* mutations cause dry eyes and dry mouth in sporadic cases with symptoms identical to those of individuals with ALSG, we screened DNA samples from 74 individuals for mutations in *FGF10*. These individuals had been evaluated and diagnosed with dry eyes and/or dry mouth, without fulfilling the criteria for Sjögren syndrome[11,12]. We found no sequence alterations in the coding region of *FGF10* in samples from these individuals,

[1]Department of Genetics and Pathology, Uppsala University, The Rudbeck laboratory, SE-751 85 Uppsala, Sweden. [2]National Oral Disability Centre and [3]Department of Pediatric Dentistry, The Institute for Postgraduate Dental Education, Box 1030, SE-551 11 Jönköping, Sweden. [4]Department of Oral Molecular Pathology, Institute of Health Bioscience, The University of Tokushima Graduate School and [5]Department of Biological Science and Technology, Faculty of Engineering, University of Tokushima, Tokushima 770-8506, Japan. [6]Department of Maxillofacial Radiology, The Institute for Postgraduate Dental Education, Box 1030, SE-551 11 Jönköping, Sweden. [7]Department of Odontology-Periodontics, Faculty of Dentistry, University of Bergen, Aarstedveien 17, N-5009 Bergen, Norway. [8]Broegelmann Research Laboratory, The Gade Institute, University of Bergen, Armauer Hansen Building, N-5021 Bergen, Norway. [9]Department of Medicine, Karolinska Institutet, SE-171 76 Stockholm, Sweden. Correspondence should be addressed to N.D. (niklas.dahl@genpat.uu.se).

Published online 16 January 2005; doi:10.1038/ng1507

© 2005 Nature Publishing Group http://www.nature.com/naturegenetics

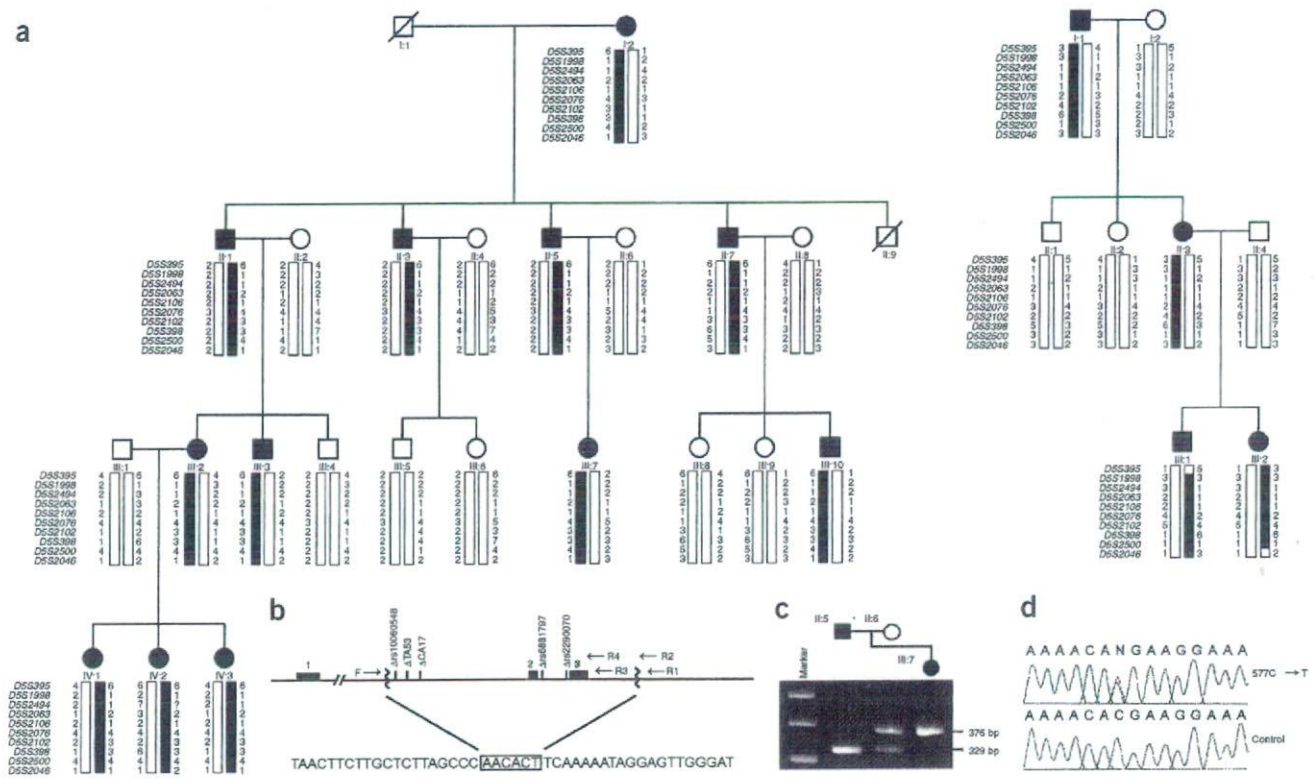

Figure 1 ALSG mapping. (**a**) Two pedigrees segregating for ALSG. Marker haplotypes on chromosome 5p13.2–5q13.1 that are linked to ALSG are indicated by black bars. (**b**) Schematic overview of *FGF10* and the 53-kb deletion inherited with ALSG in family 1 (figure not drawn to scale). Black boxes denote exons 1–3, and wavy vertical lines indicate deletion breakpoints. Genomic sequence spanning the breakpoint is shown. (**c**) Genotyping of the SNP rs6881797, located in the deletion found in family 1 and 37 bp 3′ of exon 2, by digestion with *Bsr*I. Undigested PCR product (376 bp) corresponds to the T allele and digested PCR product (329 bp) corresponds to the A allele. The absence of a paternal A allele in individual III:7 in family 1 indicates hemizygosity with respect to rs6881797. (**d**) The upper sequence chromatogram illustrates the heterozygous (R193X; 577C→T) mutation found in the affected members of family 2. The lower sequence chromatogram illustrates the corresponding normal sequence.

suggesting that mutations in *FGF10* are uncommon in individuals with unspecific sicca syndromes.

In family 1, the affected individuals are hemizygous with respect to exons 2 and 3 of *FGF10*. In family 2, the premature stop codon (R193X; 577C→T) in exon 3 predicts a truncated protein with a loss of 16 amino acids. The truncation abolishes one predicted cAMP- and cGMP-dependent protein kinase phosphorylation site (residues 194–197) and one predicted *N*-linked glycosylation site (residues 196–198)[13]. Furthermore, the truncation eliminates one of the sites for the interaction between FGF10 and fibroblast growth factor receptor 2b (FGFR2b) at residues 202 and 204 (ref. 14). If produced, the truncated FGF10 is probably unstable or nonfunctional. Both mutations in *FGF10* that we identified are consistent with the idea that haploinsufficiency with respect to FGF10 underlies ALSG.

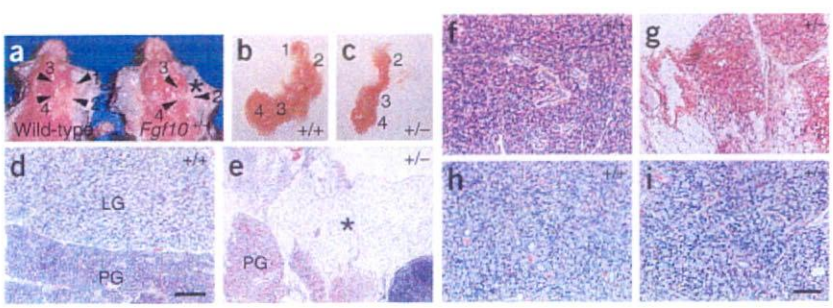

Figure 2 Salivary and lacrimal gland apparatuses of wild-type and *Fgf10*$^{+/-}$ mice. (**a**) Macroscopic examination of wild-type (left) and *Fgf10*$^{+/-}$ (right) adult mice. Ventral view of the mandibular region. 1, lacrimal; 2, parotid; 3, sublingual; 4, submandibular glands. The asterisk indicates the expected site for the lacrimal gland, which was absent in the heterozygote. Other glands were hypoplastic in the heterozygote. (**b**,**c**) Dissected salivary and lacrimal glands from the wild-type (**b**) and *Fgf10*$^{+/-}$ (**c**) mice. The salivary glands from the *Fgf10*$^{+/-}$ mouse were hypoplastic and the lacrimal gland was absent. (**d**–**i**) Histology of wild-type (**d**,**f**,**h**) and *Fgf10*$^{+/-}$ (**e**,**g**,**i**) glands. (**d**) Wild-type lacrimal (LG) and parotid (PG) glands. (**e**) The lacrimal gland was replaced by adipose tissue (asterisk) in the *Fgf10*$^{+/-}$ mouse. (**f**) Wild-type parotid gland. (**g**) Parotid gland from *Fgf10*$^{+/-}$ mouse, which appears atrophic. (**h**,**i**) Submandibular glands have similar histology in the wild type and heterozygote, as did sublingual glands (not shown). Scale bars: **d** (for panels **d** and **e**), 0.5 mm; **i** (for panels **f**–**i**), 0.1 mm.

© 2005 Nature Publishing Group http://www.nature.com/naturegenetics

The clinical examinations and medical histories of the affected family members illustrate that one intact copy of *FGF10* is sufficient for development of essential organs in humans. The restricted phenotype associated with heterozygosity with respect to *FGF10* in both humans and mice suggests that the response to FGF10 is dosage-sensitive. This is probably related to a specific embryonic stage and occurs at the site of lacrimal and salivary gland formation. A possible explanation for the absence of generalized effects in *FGF10* hemizygotes is a functional overlap with other FGFR2b ligands, such as FGF1, FGF3 and FGF7 (ref. 15).

The identification of mutations in *FGF10* as causing ALSG will hopefully result in increased diagnostic accuracy. In a larger context, this report clarifies the phenotypic effects of mutations in *FGF10* and may lead to a better understanding of the mechanisms involved in lacrimal and salivary gland formation.

We obtained informed consent from all participants in the study under a protocol approved by the Ethical Committee at Uppsala University or by the collaborating Universities.

URLs. Primer 3 is available at http://www-genome.wi.mit.edu/cgi-bin/primer/primer3_www.cgi/. The National Center for Biotechnology Information Entrez Genome Map Viewer is available at http://www.ncbi.nlm.nih.gov/mapview. The Ensembl Human Genome Server database is available at http://www.ensembl.org/. The Genome Database is available at http://www.gdb.org/.

Accession numbers. GenBank: human *FGF10*, NM_004465; human chromosome 5 clones containing *FGF10*, AC093537.2 and AC093289.2. GenBank Protein: human FGF10, NP_004456.1.

Note: Supplementary information is available on the Nature Genetics website.

ACKNOWLEDGMENTS

We thank the family members that participated in this study, N. Hagwall and M. Wyon for ophthalmologic examinations and L. Cato and Uppsala Genome Center. This work was supported by grants to N.D. from the Swedish Research Council, Swedish Cancer Society, Childrens' Cancer Foundation of Sweden, the Torsten and Ragnar Söderbergs Fund, the Borgström Foundation and Uppsala University.

COMPETING INTERESTS STATEMENT

The authors declare that they have no competing financial interests.

Received 24 August; accepted 22 December 2004
Published online at http://www.nature.com/naturegenetics/

1. Wiedemann, H.R. *Am. J. Med. Genet.* **68**, 222–224 (1997).
2. Ferreira, A.P. *et al. Am. J. Med. Genet.* **94**, 32–34 (2000).
3. Bolstad, A.I. & Jonsson, R. *Arthritis Res.* **4**, 353–359 (2002).
4. Young, W. *et al. Oral Surg. Oral Med. Oral Pathol. Oral Radiol. Endod.* **92**, 38–48 (2001).
5. Milunsky, J.M., Lee, V.W., Siegel, B.S. & Milunsky, A. *Am. J. Med. Genet.* **37**, 371–374 (1990).
6. Emoto, H. *et al. J. Biol. Chem.* **272**, 23191–23194 (1997).
7. Makarenkova, H.P. *et al. Development* **127**, 2563–2572 (2000).
8. Ohuchi, H. *et al. Biochem. Biophys. Res. Commun.* **277**, 643–649 (2000).
9. Min, H. *et al. Genes Dev.* **12**, 3156–3161 (1998).
10. Sekine, K. *et al. Nat. Genet.* **21**, 138–141 (1999).
11. Vitali, C. *et al. Arthritis Rheum.* **36**, 340–347 (1993).
12. Vitali, C. *et al. Ann. Rheum. Dis.* **61**, 554–558 (2002).
13. Bagai, S. *et al. J. Biol. Chem.* **277**, 23828–23837 (2002).
14. Yeh, B.K. *et al. Proc. Natl. Acad. Sci. USA* **100**, 2266–2271 (2003).
15. De Moerlooze, L. *et al. Development* **127**, 483–492 (2000).

© 2005 Nature Publishing Group http://www.nature.com/naturegenetics

Development of Autoimmunity against Transcriptionally Unrepressed Target Antigen in the Thymus of Aire-Deficient Mice[1]

Noriyuki Kuroda,* Tasuku Mitani,* Naoki Takeda,† Naozumi Ishimaru,‡ Rieko Arakaki,‡ Yoshio Hayashi,‡ Yoshimi Bando,§ Keisuke Izumi,§ Takeshi Takahashi,¶ Takashi Nomura,¶ Shimon Sakaguchi,¶‖ Tomoo Ueno,# Yousuke Takahama,# Daisuke Uchida,* Shijie Sun,* Fumiko Kajiura,* Yasuhiro Mouri,* Hongwei Han,* Akemi Matsushima,* Gen Yamada,† and Mitsuru Matsumoto[2]*

Autoimmune regulator (AIRE) gene mutation is responsible for the development of organ-specific autoimmune disease with monogenic autosomal recessive inheritance. Although Aire has been considered to regulate the elimination of autoreactive T cells through transcriptional control of tissue-specific Ags in thymic epithelial cells, other mechanisms of AIRE-dependent tolerance remain to be investigated. We have established Aire-deficient mice and examined the mechanisms underlying the breakdown of self-tolerance. The production and/or function of immunoregulatory T cells were retained in the Aire-deficient mice. The mice developed Sjögren's syndrome-like pathologic changes in the exocrine organs, and this was associated with autoimmunity against a ubiquitous protein, α-fodrin. Remarkably, transcriptional expression of α-fodrin was retained in the Aire-deficient thymus. These results suggest that Aire regulates the survival of autoreactive T cells beyond transcriptional control of self-protein expression in the thymus, at least against this ubiquitous protein. Rather, Aire may regulate the processing and/or presentation of self-proteins so that the maturing T cells can recognize the self-Ags in a form capable of efficiently triggering autoreactive T cells. With the use of inbred Aire-deficient mouse strains, we also demonstrate the presence of some additional factor(s) that determine the target-organ specificity of the autoimmune disease caused by Aire deficiency. *The Journal of Immunology,* **2005, 174: 1862–1870.**

Autoimmune diseases are mediated by sustained adaptive immune responses specific for self-Ags through unknown mechanisms. Although breakdown of self-tolerance is considered to be the key event in the disease process, the mechanisms that allow the production of auto-Abs and/or autoreactive lymphocytes are largely enigmatic (1). The situation seems to have become more complicated due to the existence of multiple factors that influence the disease process, such as environmental factors, immune dysregulation, and genetic predisposition. In this regard, although only a small number of genes genetically relevant to the pathogenetic processes for the development of autoimmune diseases have been found so far (2), genetic engineering of such genes in mice should enable us to establish disease models and facilitate an understanding of the disease mechanisms to a large extent. One of these genes is the autoimmune regulator (*AIRE*)[3] mutation, which is responsible for the development of autoimmune-polyendocrinopathy-candidiasis ectodermal dystrophy (APECED; Online Mendelian Inheritance in Man 240300) with autosomal recessive inheritance (3–6).

The *AIRE* gene encodes a predicted 58-kDa protein carrying a conserved nuclear localization signal, two plant homeodomain (PHD)-type zinc fingers, four LXXLL motifs or nuclear receptor interaction domains, and the recently described homogeneously staining region (HSR) and SAND domains (3, 4); the HSR and SAND domains have been suggested to function in homodimerization and DNA binding, respectively (7, 8). Based on the fact that PHD resembles the RING finger, which can function as an E3 ubiquitin ligase, in both sequence and structure (9), we have recently found that AIRE acts as an E3 ubiquitin ligase through the N-terminal PHD domain (PHD1) (10). Because the ubiquitin-proteasome pathway plays an essential role in diverse cell functions such as cell cycle progression, signal transduction, cell differentiation, DNA repair and apoptosis (11, 12), we speculate that AIRE should play a fundamental role by facilitating polyubiquitinylation of the substrate(s) in yet undetermined processes. The significance

*Division of Molecular Immunology, Institute for Enzyme Research, University of Tokushima, Tokushima, Japan; †Center for Animal Resources and Development, and Graduate School of Molecular and Genomic Pharmacy, Kumamoto University, Kumamoto, Japan; ‡Department of Pathology, Tokushima University School of Dentistry, Tokushima, Japan; §Department of Molecular and Environmental Pathology, School of Medicine, University of Tokushima, Tokushima, Japan; ¶Department of Experimental Pathology, Institute for Frontier Medical Sciences, Kyoto University, Kyoto, Japan; ‖Laboratory for Immunopathology, RIKEN Research Center for Allergy and Immunology, Yokohama, Japan; and #Division of Experimental Immunology, Institute for Genome Research, University of Tokushima, Tokushima, Japan

Received for publication August 20, 2004. Accepted for publication November 17, 2004.

The costs of publication of this article were defrayed in part by the payment of page charges. This article must therefore be hereby marked *advertisement* in accordance with 18 U.S.C. Section 1734 solely to indicate this fact.

[1] This work was supported in part by Special Coordination Funds of the Ministry of Education, Culture, Sports, Science and Technology, the Japanese Government (MEXT), and by a grant-in-aid for Scientific Research from the MEXT.

[2] Address correspondence and reprint requests to Dr. Mitsuru Matsumoto, Division of Molecular Immunology, Institute for Enzyme Research, University of Tokushima, 3-18-15 Kuramoto, Tokushima 770-8503, Japan. E-mail address: mitsuru@ier.tokushima-u.ac.jp

[3] Abbreviations used in this paper: AIRE, autoimmune regulator; APECED, autoimmune-polyendocrinopathy-candidiasis ectodermal dystrophy; TEC, thymic epithelial cell; mTEC, medullary TEC; PHD, plant homeodomain; HEL, hen egg lysozyme; 3d-Tx mice, mice thymectomized 3 days after birth; SS, Sjögren's syndrome; Treg, immunoregulatory T cell; BM, bone marrow.

Copyright © 2005 by The American Association of Immunologists, Inc.

0022-1767/05/$02.00

of this finding was underscored by the fact that disease-causing missense mutations in PHD1 abolished its E3 ligase activity (10).

One important aspect of AIRE, in the context of autoimmunity, is its limited tissue expression in medullary thymic epithelial cells (mTEC) and cells of the monocyte-dendritic cell lineage of the thymus (13, 14). Both cell types are considered to play major roles in the establishment of self-tolerance by eliminating autoreactive T cells (negative selection) (1, 15) and/or by producing immunoregulatory T cells (Tregs), which prevent $CD4^+$ T cell-mediated organ-specific autoimmune diseases (16, 17). For this purpose, thymic epithelial cells (TECs) have been postulated to express a set of self-Ags encompassing all of the self-Ags expressed by parenchymal organs. Supporting this hypothesis, analysis of gene expression in the thymic stroma has demonstrated that mTECs are a specialized cell type in which promiscuous expression of a broad range of peripheral tissue-specific genes is an autonomous property (18). Aire in TECs has been suggested to regulate this promiscuous gene expression (19).

Fundamental roles of Aire in the elimination of autoreactive T cells in vivo have been demonstrated by the use of a TCR-transgenic mouse system (20). Mice expressing hen egg lysozyme (HEL) in pancreatic β cells driven by the rat insulin promoter were crossed with mice expressing TCR specific for HEL, and the fate of HEL-specific T cells was monitored in either the presence or absence of Aire. Remarkably, Aire-deficient TCR-transgenic mice showed almost complete failure to delete the autoreactive (i.e., HEL specific) T cells in the thymus (20). Because Aire-deficient mTEC showed a reduction in transcription of a group of genes encoding peripheral Ags analyzed by the gene-chip technique (19), it has been hypothesized that pathogenic autoreactive T cells could not be eliminated efficiently due to the reduced expression of corresponding target Ags in the Aire-deficient thymus (20). However, as this transgenic study did not demonstrate the effect of Aire loss on the thymic expression of HEL, there is still a lack of experimental evidence to connect the postulated roles of Aire in the transcriptional regulation of tissue-specific Ag expression with efficient elimination of autoreactive T cells. Thus, beyond transcriptional control of self-Ags in the thymus, other mechanisms of AIRE-dependent tolerance remain to be investigated. Furthermore, the effect of Aire deficiency on the production and/or function of Tregs has not yet been fully documented (19–21). Finally, the factors contributing to the complexity of the APECED phenotype (i.e., involvement of various target organs among patients) are unknown. Although intrafamilial variation in the clinical pictures suggests that factors other than the specific *AIRE* mutations might be involved in the disease process (22), this hypothesis cannot be easily proven in human subjects. To approach these issues, we have generated Aire-deficient mice by gene targeting. Identification of a target Ag associated with the tissue destruction caused by Aire deficiency together with strain-dependent target-organ specificity of the autoimmune disease has suggested unique properties of AIRE in the establishment and maintenance of self-tolerance.

Materials and Methods

Mice

Aire-deficient mice were generated by gene targeting. Briefly, the targeting vector was constructed by replacing the genomic *Aire* locus starting from exon 5 to exon 12 with the neomycin resistance gene (neo^r). The targeting vector was introduced into TT2 embryonic stem cells ($H\text{-}2^{b/k}$) (23), and the homologous recombinant clones were first identified by PCR and confirmed by Southern blot analysis. After the targeted cells had been injected into ICR 8 cell embryos (CLEA Japan), the resulting chimeric male mice were mated with C57BL/6 females to establish the germline transmission. C57BL/6 mice, BALB/c mice, and BALB/cA Jcl-ν mice were purchased from CLEA Japan. The mice were maintained under pathogen-free conditions and handled in accordance with the Guidelines for Animal Experimentation of Tokushima University School of Medicine. The experiments were initiated when the mice were 8–12 wk of age.

Pathology

Formalin-fixed tissue sections were subjected to H&E staining, and two pathologists independently evaluated the histology without being informed of the condition of each individual mouse. Histological changes were scored as 0 (no change), 1 (mild lymphoid cell infiltration), or 2 (marked lymphoid cell infiltration).

Measurement of tear secretion

Measurement of tear secretion was performed as previously described (24, 25). Briefly, anesthetized mice were injected i.p. with 100 μl of pilocarpine hydrochloride (1 mg/ml) to stimulate tear production. Secreted tears were absorbed every 5 min with a cotton thread treated with a pH indicator phenol red (ZONE-QUICK; Menicon), and the length of the red portion of the thread was measured each time. Total length of the red portion of the thread during the first 20 min after pilocarpine injection was normalized by body weight.

ELISA and Western blot analysis

Various forms of recombinant α-fodrin were expressed with pGEX-4Ts plasmids (26). Western blot analysis and ELISA for the detection of auto-Abs against various forms of recombinant α-fodrin were performed with anti-mouse IgG Ab (Vector Laboratories), as described previously (25, 27–31). For the ELISA, absorbance values greater than the mean $\pm$ 3 SD in wild-type sera were considered positive. Western blot analysis of α-fodrin expression from the proteins extracted from the thymus and lacrimal glands was performed with mouse anti-α-fodrin mAb (Affiniti) and rabbit anti-AFN-A polyclonal Ab (25, 27–31).

Autoreactive responses against α-fodrin

For in vitro stimulation with α-fodrin, total splenocytes were stimulated with 10 μg/ml recombinant α-fodrin. For the last 8 h of the 32-h culture period, the cells were pulsed with [^{3}H]thymidine, and ^{3}H incorporation was determined as described previously (25).

Thymic stroma preparation

Thymic stroma was prepared as described previously with slight modification (32). Briefly, thymic lobes were isolated from three mice for each group and cut into small pieces. The fragments were gently rotated in RPMI 1640 medium (Invitrogen) supplemented with 10% heat-inactivated FCS (Invitrogen), 20 mM HEPES, 100 U/ml penicillin, 100 μg/ml streptomycin, and 50 μM 2-ME, hereafter referred to as R10, at 4°C for 30 min, and dispersed further with pipetting to remove the majority of thymocytes. The resulting thymic fragments were digested with 0.15 mg/ml collagenase IV (Sigma-Aldrich) and 10 U/ml DNase I (Roche Molecular Biochemicals) in RPMI 1640 at 37°C for 15 min. The supernatants that contained dissociated TECs were saved, whereas the remaining thymic fragments were further digested with collagenase IV and DNase I. This step was repeated twice, and the remaining thymic fragments were digested with collagenase IV, DNase I, and 0.1 mg/ml dispase I (Roche Applied Science) at 37°C for 30 min. The supernatants from this digest were combined with the supernatants from the collagenase digests, and the mixture was centrifuged for 5 min at 450 $\times$ *g*. The cells were suspended in PBS containing 5 mM EDTA and 0.5% FCS and kept on ice for 10 min. $CD45^-$ thymic stromal cells were then purified by depleting $CD45^+$ cells with MACS CD45 microbeads (Miltenyi Biotec) according to the manufacturer's instructions. The resulting preparations contained ~60% Ep-CAM^+ cells and <10% thymocytes (i.e., CD4/CD8 single-positive and CD4/CD8 double-positive cells), as determined by flow cytometric analysis.

RT-PCR

RNA was extracted from thymic stromal cells with High Pure RNA isolation kit (Roche Applied Science) and made into cDNA with cDNA Cycle kit (Invitrogen) according to the manufacturer's instructions. The following primer pairs for the *α-fodrin* gene were used: 5′-GCTTCAAGGAG CTCTCTACC-3′ and 5′-GCAGTTTGATTCCTTTCTCC-3′ (encompassing *α-fodrin* exons 1–3; accession no. XM_355324), 5′-CCAGCAGCAA CAATTTAATC-3′ and 5′-AGCAGATTCTGGACTCCAAT-3′ (encompassing the *α2-spectrin* exons 2–4; accession no. XM_207079), and 5′-GTG CAGAAATCAGCTGAGAA-3′ and 5′-GCTTGTGTTTCTTCCTCAGA-3′ (encompassing the *α2-spectrin* exons 24–27). PCR was conducted in a final volume of 20 μl with 1.5 U of ExTaq DNA polymerase (Takara Biomedicals)

and 250 nM each primer. Cycling conditions comprised a single denaturing step at 94°C for 10 min followed by 35 cycles of 94°C for 30 s, 60°C for 30 s, and 72°C for 1.5 min, followed by a final extension step of 72°C for 10 min. For *β-actin*, a single denaturing step at 94°C for 3 min was followed by 25 cycles of 94°C for 45 s, 50°C for 45 s, and 72°C for 1 min, followed by a final extension step of 72°C for 3 min (33).

Real-time PCR

Real-time PCR for quantification of *α-fodrin*, *Foxn1*, and tissue-specific Ag genes was conducted with thymic stroma cDNA prepared as described above. The primers and the probes are as follows. *α2-spectrin* primers: 5′-GACAGCCAGTGATGAGTCATACAAG-3′ and 5′-CACGGATTCG-GTCAGCATT-3′; *α2-spectrin* probe: 5′-FAM-ACCCCACCAACATCC AGAGCAAGC-3′; *Foxn1* primers: 5′-GACATGCACCTCAGCACTCT CTA-3′ and 5′-CTGATGTTGGGCATAGCTCAAG-3′; *Foxn1* probe: 5′-FAM- CCCGGCTCAAAGCCATTGGCTC-3′; *insulin* primers: 5′-AGA CCATCAGCAAGCAGGTC-3′ and 5′-CTGGTGCAGCACTGATCCAC-3′; *insulin* probe: 5′-FAM-CCCGGCAGAAGCGTGGCATT-3′; *salivary protein 1* primers: 5′-ACTCCTTGTGTTGCTTGGTGTTT-3′ and 5′-TCGACTGAATCAGAGGAATCAACT-3′; *salivary protein 1* probe: 5′-FAM-TTCACCAGCAGAATCAGCAGTTCCAGAA; *C-reactive protein* primers: 5′-TACTCTGGTGCCTTCTGATCATGA-3′ and 5′-GGCTTC TTTGACTCTGCTTCCA-3′; *C-reactive protein* probe: 5′-FAM-C AGCTTCTCTCGGACTTTTGGTCATGA-3′; *fatty acid binding protein* primers: 5′-CGTGTAGACAATGGAAAGGAGCT-3′ and 5′-AA GAATCGCTTGGCCTCAACT-3′; *fatty acid binding protein* probe: 5′-FAM-TCATTACCAGAAACCTCTCGGACAGCA-3′; *glutamic acid decarboxylase 67* primers: 5′-TCCTCCAAGAACCTGCTTTCC-3′ and 5′-GCTCCTCCCCGTTCTTAGCT-3′; *glutamic acid decarboxylase 67* probe: 5′-FAM-CCGACTTCTCCAACCTGTTTGCTCAAGA-3′. *Foxp3* expression was examined with cDNAs prepared from splenocytes ($CD4^+CD25^+$ or $CD4^+CD25^-$) and total thymus. The primers, the probes, and the reactions used for *Foxp3* and *Hprt* were those described previously (33, 34).

Thymus grafting

Thymus grafting was performed as previously performed (33). Briefly, thymic lobes were isolated from embryos at 14.5 days postcoitus, and then cultured for 4 days on Nucleopore filters (Whatman) placed on R10 containing 1.35 mM 2′-deoxyguanosine (Sigma-Aldrich). Five pieces of thymic lobes were grafted under the renal capsule of BALB/c *nude* mice. After 6–8 wk, reconstitution of peripheral T cells was determined by flow cytometric analysis with anti-CD4 (clone GK1.5; BD Pharmingen) and anti-CD8 (clone 53-6.7; BD Pharmingen) mAbs, and then the thymic chimeras were used for analysis.

Immunohistochemistry

Immunohistochemical analysis of the thymus was performed as described previously (35, 36). For the detection of auto-Abs, mouse serum was incubated with various organs obtained from Rag2-deficient mice. FITC-conjugated anti-mouse IgG Ab (Southern Biotechnology Associates) was used for the detection (33).

Isolation and functional analysis of Tregs

Spleen cell suspensions were stained with FITC-conjugated anti-CD25 (clone 7D4) and PE-conjugated anti-CD4 (clone H129.19) (BD Pharmingen), and sorted by FACS (ALTRA; Beckman Coulter) as described previously (37). The purity of the $CD25^-$ and $CD25^+CD4^+$ populations was >90 and 95%, respectively. Spleen cells sorted as described above were cocultured with RBC-lysed and irradiated (15 Gy) spleen cells (5×10^4) from wild-type mice as APC for 3 days in 96-well round-bottom plates in R10. Anti-CD3 mAb (clone 145-2C11) (Cedarlane Laboratories) at a final concentration of 10 μg/ml was added to the culture for stimulation, and ^3H incorporation during the last 6 h of culture was measured.

Results

Development of Sjögren's syndrome (SS)-like pathologic changes in exocrine organs from Aire-deficient mice

To investigate the roles of AIRE in the establishment and maintenance of self-tolerance in vivo, we generated Aire-null mutant mice. To this end, we deleted a large proportion of the known functional domains of *Aire* including SAND, PHD1, and PHD2 (6) (Fig. 1*A*). The correct targeted event was confirmed by Southern blot analysis and genomic PCR of material from the gene-targeted

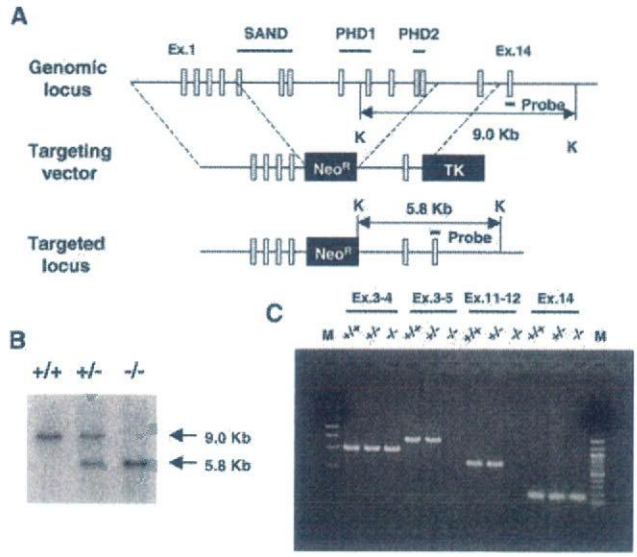

FIGURE 1. Generation of Aire-deficient mice. *A*, Targeted disruption of the gene encoding *Aire* by homologous recombination. K, *Kpn*I restriction site. *B*, Southern blot analysis of genomic DNA from offspring of heterozygous Aire-deficient mouse intercrosses. Tail DNA was digested with *Kpn*I and hybridized with a probe shown in *A*. *C*, Detection of genomic fragments of the *Aire* locus by PCR. Sequences spanning exons 5 and 12 were not amplified in tail DNA of homozygous Aire-deficient mice.

mice (Fig. 1, *B* and *C*). Offspring homozygous for Aire deficiency were born in the numbers expected from the heterozygous crossing, and homozygous Aire-deficient mice were grossly normal. Although both male and female homozygous Aire-deficient mice are fertile when crossed with wild-type mice, homozygous crossing produced offspring only occasionally (F. Kajiura and M. Matsumoto, unpublished observation). Total spleen cell numbers and total thymocyte numbers were indistinguishable between control and Aire-deficient mice. Flow cytometric analysis showed similar expression of B220, CD3, CD4, and CD8 in the spleen and thymus of control and Aire-deficient mice. Proliferative responses and Ig production from the B cells after various stimuli, and proliferative responses and IL-2 production from the T cells stimulated with anti-CD3 mAb, were also unchanged by the Aire deficiency (S. Sun and M. Matsumoto, unpublished observation).

To assess the impact of Aire deficiency on the breakdown of self-tolerance, we inspected various organs (i.e., salivary glands, lacrimal glands, thyroid, heart, lung, liver, stomach, pancreas, kidney, small intestine, testis, and ovary) from Aire-deficient mice of original mixed background (i.e., $H\text{-}2^{b/k} \times H\text{-}2^b$). The most marked changes were evident in the lacrimal glands (Fig. 2, *A* and *B*); all the Aire-deficient mice showed infiltration of many lymphoid cells in the lacrimal glands, whereas no such changes were observed in the control mice. We also observed infiltration of many lymphoid cells in the parotid glands (8 of 8 Aire-deficient mice) and submandibular glands (10 of 16 Aire-deficient mice) (Fig. 2*A*). Consistent with these SS-like pathologic changes in exocrine organs from Aire-deficient mice, secretion of tears per unit of mouse body weight was decreased in the affected mice (0.89 ± 0.33 mm/20 min/body weight (g) from control mice ($n = 5$) vs 0.46 ± 0.08 mm/20 min/body weight (g) from Aire-deficient mice ($n = 4$); $p < 0.05$). In 1 of 10 Aire-deficient mice, lymphoid cell infiltration in either the stomach or pancreas was also observed. There were no obvious pathologic changes in other organs from Aire-deficient mice during follow-up to the age of 8 mo.

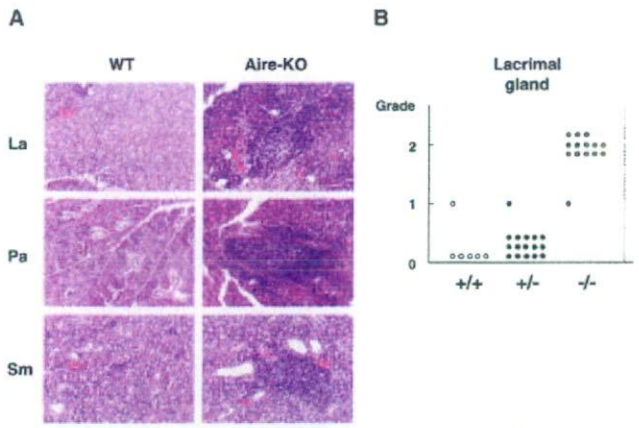

FIGURE 2. Development of organ-specific pathologic changes in Aire-deficient mice. *A*, Aire-deficient mice exhibited many infiltrating lymphoid cells in the lacrimal gland (La), parotid gland (Pa), and submandibular gland (Sm). In contrast, these changes were scarcely observed in control mice. Original magnification, ×100. *B*, Histological changes in H&E-stained tissue sections were scored as 0 (no change), 1 (mild lymphoid cell infiltration), or 2 (marked lymphoid cell infiltration). One mark corresponds to one mouse analyzed.

Autoreactive responses against α-fodrin in Aire-deficient mice

We have previously reported that NFS/*sld* mutant mice thymectomized 3 days after birth (3d-Tx) exhibit SS-like phenotypes with autoreactivity against α-fodrin, a ubiquitously expressed actin-binding protein (27, 38). Because of the similarity of SS-like phenotypes between Aire-deficient mice and the 3d-Tx-SS model, we investigated whether Aire-deficient mice exhibit autoreactivity against α-fodrin. We first tested the production of auto-Ab against various forms of recombinant α-fodrin in sera from Aire-deficient mice using Western blot analysis (Fig. 3, *A* and *B*). Sera from 3d-Tx mice showed reactivity predominantly against the JS-1 fragment (27). Four of five Aire-deficient mice showed reactivity against 2.7A, and two mice showed reactivity against 3′DA (Fig. 3*B*). Sera from control mice showed no such reactivities. Production of auto-Ab against α-fodrin in Aire-deficient mice was also evaluated by ELISA using additional forms of recombinant α-fodrin (31) and larger numbers of mice. Ten of 11 Aire-deficient mice showed significantly higher reactivities against at least one form of recombinant α-fodrin fragment compared with those from 11 control mice (Fig. 3*C*). Interestingly, each Aire-deficient mouse showed reactivity against different forms of α-fodrin.

We also confirmed the development of autoimmunity against α-fodrin using splenocytes from Aire-deficient mice (25). Such splenocytes cultured with recombinant α-fodrin showed significant proliferative responses; four Aire-deficient mice tested showed a response to 2.7A, but not to JS-1, whereas no such reactivities were observed from age-matched control mice (Fig. 4).

Unrepressed expression of corresponding target Ag in Aire-deficient thymus

The mechanism controlling the thymic microenvironment necessary for the establishment of self-tolerance in an Aire-dependent manner is of considerable interest. It has been suggested that "promiscuous" expression of a broad range of peripheral tissue-specific genes by TECs is essential for establishing self-tolerance (18), and Aire has been implicated in the control of this promiscuous gene expression through a transcriptional mechanism (19). Supporting this notion, real-time PCR has revealed that expression of *insulin*

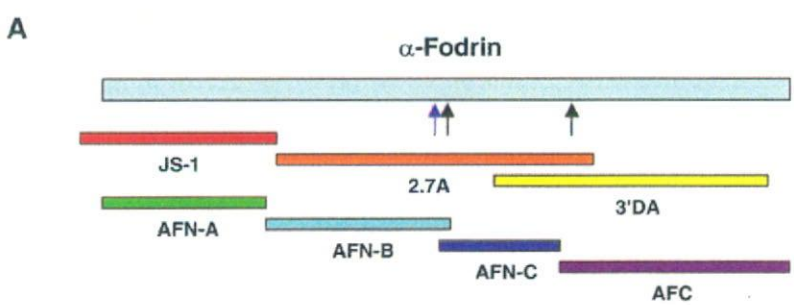

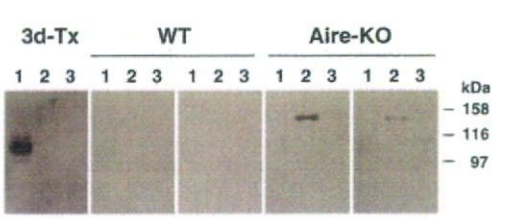

C

	JS-1	2.7A	3'DA	AFN-A	AFN-B	AFN-C	AFC
KO 1	0.052	0.196	0.081	0.053	0.435	0.088	0.074
2	0.620	0.171	0.034	0.043	0.227	0.076	0.066
3	0.084	0.094	0.050	0.099	0.089	0.051	0.167
4	0.186	0.058	0.058	0.093	0.187	0.047	0.213
5	0.043	0.057	0.037	0.059	0.103	0.105	0.110
6	0.028	0.027	0.057	0.023	0.055	0.045	0.081
7	0.339	0.095	0.035	0.050	0.082	0.207	0.072
8	0.178	0.034	0.034	0.071	0.062	0.044	0.076
9	0.084	0.178	0.037	0.079	0.259	0.054	0.307
10	0.053	0.083	0.865	0.020	0.136	0.038	0.796
11	0.264	0.060	0.046	0.151	0.103	0.185	0.075

FIGURE 3. Production of auto-Abs against α-fodrin in Aire-deficient mice. *A*, Schematic representation of α-fodrin. Black arrows and a blue arrow show the sites of cleavage by caspase 3 and calpain, respectively. *B*, Western blot analysis for recombinant α-fodrin with Aire-deficient mouse sera. Representative results from two mice from both wild-type and Aire-deficient mice are shown. Serum from NFS/*sld* mutant 3d-Tx mice reacted predominantly with the JS-1 fragment. 1, JS-1; 2, 2.7A; 3, 3′DA. *C*, Detection of auto-Abs against various forms of α-fodrin in sera from Aire-deficient mice using ELISA. Absorbance values greater than the mean ± 3 SD in wild-type mouse sera were considered positive and are colored.

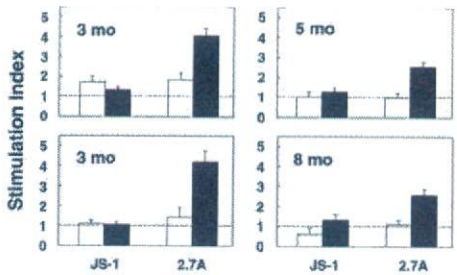

FIGURE 4. Autoreactive responses against α-fodrin by splenocytes from Aire-deficient mice. Proliferative responses of total splenocytes against two forms of recombinant α-fodrin (shown in Fig. 3*A*) were determined, and stimulation indices are demonstrated from control mice (open bars) and Aire-deficient mice (filled bars). Ages of the mice used are indicated.

and *salivary protein 1* was significantly reduced in the Aire-deficient thymic stroma (Fig. 5*A*). Because Aire-deficient mice developed autoimmunity against the defined target Ag, α-fodrin, we examined whether the expression of α-fodrin mRNA in the thymic stroma is changed in Aire-deficient mice. Using real-time PCR together with semiquantitative RT-PCR with three sets of primers encompassing the entire coding region of *α-fodrin*, we detected unrepressed *α-fodrin* expression from Aire-deficient thymic stroma when compared with that from control thymic stroma (Fig. 5, *A* and *B*); this was observed under the condition where the expression of *Foxn1*, which encodes a transcription factor involved in thymus development (39), was indistinguishable between the samples (Fig. 5*A*). Thus, our results suggest that Aire regulates self-tolerance beyond the transcriptional control of self-protein expression in the thymus, at least against this ubiquitously expressed protein.

To test whether autoreactivity against α-fodrin is associated with the development of inflammatory lesions in exocrine organs from Aire-deficient mice, we performed Western blot analysis using proteins extracted from the lacrimal glands. Both lacrimal glands and thymus from younger Aire-deficient mice (i.e., 3 mo) contained larger quantities of intact form α-fodrin (240 kDa) than the cleaved form (150 kDa), as observed for proteins from the control mice (Fig. 6*A*); this was demonstrated with two different kinds of Abs recognizing the C-terminal half (anti-α-fodrin mAb) and N-terminal half (anti-AFN-A polyclonal Ab) of α-fodrin. However, lacrimal glands from some aged Aire-deficient mice (i.e., 8 mo) contained a reduced amount of the intact form (Fig. 6*B*), although no detectable changes in α-fodrin expression in the thymus were observed in either form or quantity. This result suggests that autoreactivity against α-fodrin is associated with the pathogenetic process responsible for destruction of the lacrimal glands in this SS-like model, as observed in 3d-Tx-SS model (27, 38).

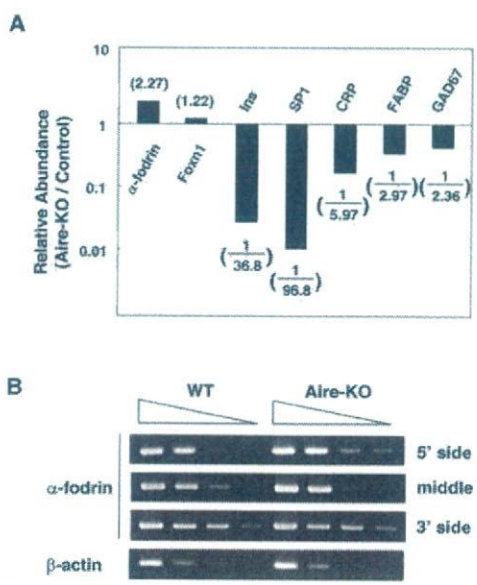

FIGURE 5. Unrepressed target Ag expression from Aire-deficient thymus. *A*, Real-time PCR for *α-fodrin*, *Foxn1*, and peripheral tissue-specific genes (i.e., Ins, *insulin*; SP1, *salivary protein 1*; CRP, *C-reactive protein*; FABP, *fatty acid-binding protein*; GAD67, *glutamic acid decarboxylase 67*) was performed using thymic-stroma RNAs from control and Aire-deficient mice. *Hprt* expression level was used as an internal control. Relative abundance of each gene was calculated from the ratio between the values from control thymus and those from Aire-deficient thymus (e.g., *insulin/Hprt* value from Aire-deficient mice was divided by *insulin/Hprt* value from control mice) and is shown in parentheses. One representative result from a total of three repeats is shown. *B*, Semiquantitative RT-PCR for *α-fodrin* was performed using thymic-stroma RNAs from control and Aire-deficient mice. *β-Actin* was used to verify equal amounts of RNAs in each sample. Three sets of primers encompassing the entire coding region of *α-fodrin* were used for detection. One representative result from a total of three repeats is shown.

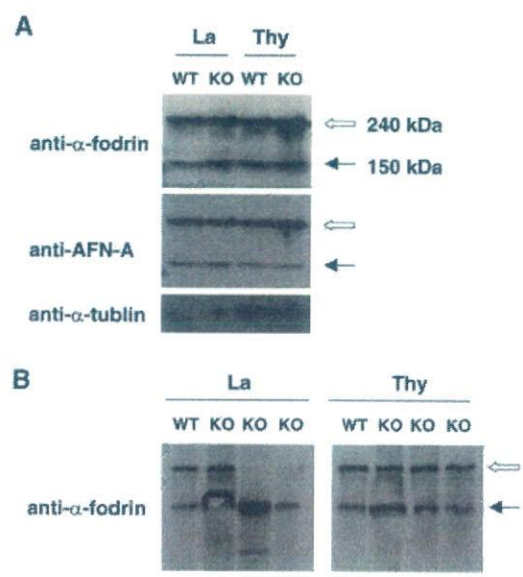

FIGURE 6. Autoreactivity against α-fodrin is associated with the pathogenetic process responsible for destruction of the lacrimal glands. *A*, Proteins extracted from the lacrimal glands and thymus of 3-mo-old mice were subjected to Western blot analysis using two different kinds of Abs recognizing the C-terminal half (anti-α-fodrin Ab, *top*) and N-terminal half (anti-AFN-A Ab, *center*) of α-fodrin. Open and filled arrows indicate the 240-kDa intact form and 150-kDa cleaved form of α-fodrin, respectively. The same blot was probed with anti-α-tubulin Ab (*bottom*). La, lacrimal gland; Thy, thymus. *B*, Proteins were extracted from the lacrimal glands and thymus of 8-mo-old mice. Western blot analysis was performed as shown in *A*. Lacrimal glands from some of the Aire-deficient mice showed a markedly reduced amount of the intact form (*left panel*, third and fourth lanes), although Aire-deficient thymus showed no detectable changes in α-fodrin expression in terms of form or quantity compared with control thymus (*right panel*). Open and filled arrows indicate the 240-kDa intact form and 150-kDa cleaved form of α-fodrin, respectively.

Loss of Aire in the thymic stroma is responsible for the breakdown of self-tolerance

Despite the predominant Aire expression in TECs, thymic structure was not apparently affected by the absence of Aire. Results of H&E staining as well as immunohistochemistry with the lectin *Ulex europaeus* agglutinin 1 (40) and ER-TR5 mAb (41), both recognizing a subset of mTEC, were indistinguishable between control and Aire-deficient mice (F. Kajiura, T. Ueno, Y. Takahama, and M. Matsumoto, unpublished observation). Organization of dendritic cells in the thymus identified with the mAb CD11c was also unaffected by Aire deficiency. Thus, Aire may not affect thymic organogenesis. Alternatively, relatively low frequencies of Aire-expressing cells among mTECs may account for the apparently normal thymic structure in Aire-deficient mice.

To investigate the impact of Aire deficiency in the thymic microenvironment, we generated thymic chimeras. Thymic lobes were isolated from control and Aire-deficient embryos of mixed background (H-$2^{b/k}$ × H-2^{b}) and cultured for 4 days in the presence of 2′-deoxyguanosine to eliminate thymocytes. Such thymic lobes did not contain any live thymocytes, as determined by flow cytometric analysis and Western blot analysis with anti-lck Ab (33). The lobes were then grafted under the renal capsule of BALB/c *nude* mice (H-2^{d}). Grafting of both control and Aire-deficient embryonic thymus induced T cell maturation in BALB/c *nude* mice at the periphery to a similar extent: $CD4^+$ T cells plus $CD8^+$ T cells were 12.5 ± 2.2% in *nude* mice grafted with control thymus (n = 6), compared with 12.3 ± 1.6% in *nude* mice grafted with Aire-deficient thymus (n = 7). It is important to note that the mature T cells produced de novo in both cases originated from Aire-sufficient *nude* mouse bone marrow (BM). Remarkably, histological examination of Aire-deficient thymus-grafted mice revealed infiltration of many lymphoid cells in the liver (mainly in the portal area) and pancreas (interlobular periductal and perivascular areas near islets) (Fig. 7, *A* and *B*). In contrast, we observed few such changes in control thymus-grafted mice.

To confirm that T cells developing in a thymic microenvironment without Aire are autoreactive per se, we injected splenocytes obtained from BALB/c *nude* mice grafted with Aire-deficient thymus into another group of BALB/c *nude* mice. We observed similar lymphoid cell infiltration in the liver of the recipient mice, whereas injection of splenocytes obtained from *nude* mice grafted with control thymus induced no such changes in the recipient mice (Fig. 7*B*). These results clearly indicate the significance of Aire as a thymic stromal element required for the establishment of self-tolerance.

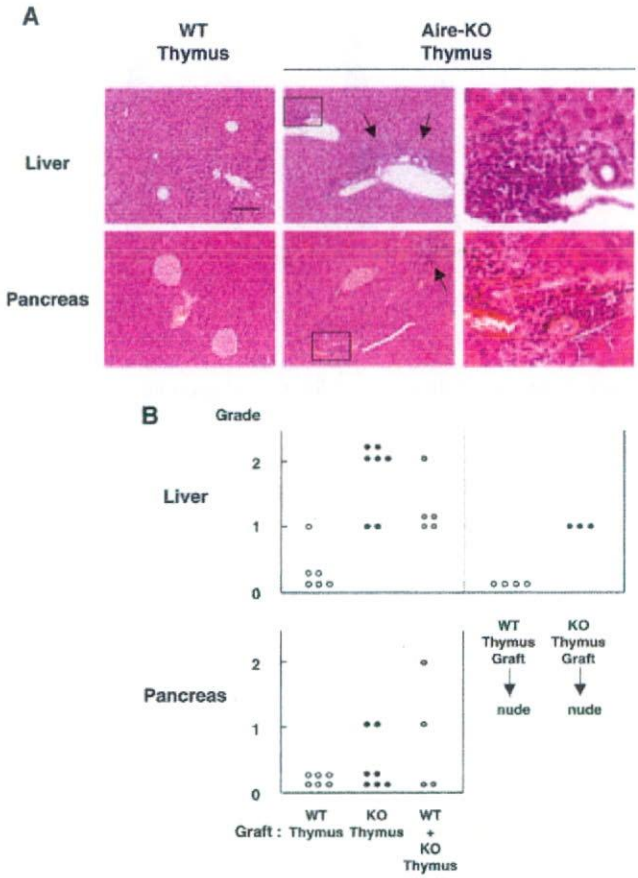

FIGURE 7. Thymic stromal elements in Aire-deficient mice are responsible for the development of autoimmunity. *A*, BALB/c *nude* mice grafted with Aire-deficient embryonic thymus (*middle panels*), but not with control embryonic thymus (*left panels*), developed an autoimmune disease phenotype in the liver and pancreas. The indicated areas are magnified in the *right panels*. Arrows indicate lymphoid cell infiltration. The scale bar corresponds to 100 μm. *B*, Many Aire-deficient thymus-grafted BALB/c *nude* mice exhibited lymphoid cell infiltration in the liver (*top*) and pancreas (*bottom*). In contrast, such changes were scarcely observed in mice grafted with control thymus. BALB/c *nude* mice grafted with both Aire-deficient thymus and control thymus showed significant pathological changes. Injection of splenocytes from BALB/c *nude* mice grafted with Aire-deficient thymus, but not with control thymus, into another group of BALB/c *nude* mice induced lymphoid cell infiltration in the liver of the recipient mice. Histological changes in H&E-stained tissue sections were scored as shown in Fig. 2*B*. One mark corresponds to one mouse analyzed.

Impaired regulation of autoreactivity in the absence of Aire

There is accumulating evidence that T cell-mediated dominant control of autoreactive T cells represents an important mechanism for the maintenance of immunologic self-tolerance (16, 17). We investigated whether loss of Aire in the thymus has a major impact on the production and/or function of Tregs. Spleen and thymus from adult Aire-deficient mice contained similar percentages as well as total numbers of $CD4^+CD25^+$ T cells compared with those from control mice (Fig. 8*A*). Real-time PCR for quantification of *Foxp3* mRNA (34, 42, 43) did not show any reduction of Tregs in the spleen of Aire-deficient mice (Fig. 8*B*). Expression of *Foxp3* in the whole thymus was also comparable between control mice and Aire-deficient mice (*Foxp3*/*Hprt* from wild-type mice = 1.8 vs *Foxp3*/*Hprt* from Aire-deficient mice = 2.4).

Recently, it has been demonstrated that functional alterations of Tregs could contribute to the development of autoimmune disease. A significant decrease in the effector function of $CD4^+CD25^+$ T cells from peripheral blood of patients with multiple sclerosis has been reported (44). It is of particular interest that the suppressor function of $CD4^+CD25^+$ T cells has been demonstrated to be defective in patients with autoimmune polyglandular syndrome type II, which is phenotypically closely related to APECED (also called autoimmune polyglandular syndrome type I) but whose pathogenesis is currently unknown (45). It is therefore important to test the function of Tregs from Aire-deficient mice. $CD4^+CD25^+$ T cells isolated from Aire-deficient mice dose-dependently suppressed [^{3}H]thymidine uptake by naive T cells cocultured in vitro with an efficiency nearly identical to that of $CD4^+CD25^+$ cells from control mice (Fig. 8*Ca*). This was also the case when responder cells ($CD4^+CD25^-$ cells) isolated from Aire-deficient mice were used for the assay (Fig. 8*Cb*). Thus, Aire does not have a major impact on the production and/or function of Tregs, at least as assessed in those assays.

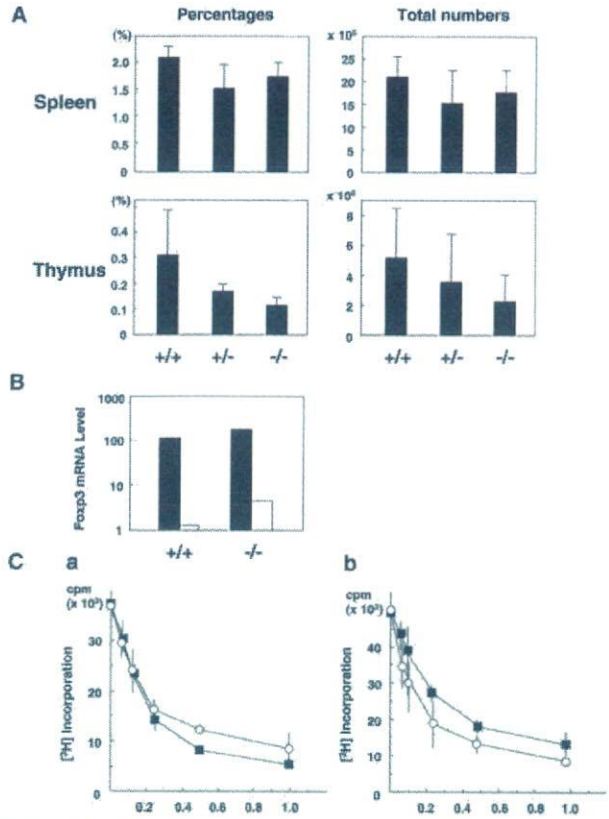

FIGURE 8. Retained production and function of Tregs from Aire-deficient mice. *A*, Spleens and thymuses from Aire-deficient mice contained percentages as well as total numbers of $CD4^+CD25^+$ T cells indistinguishable from those of control mice. $n = 5$, not statistically significant. *B*, Real-time PCR for *Foxp3* expression was performed using RNAs extracted from purified $CD4^+CD25^+$ (filled bars) and $CD4^+CD25^-$ T cells (open bars) with *Hprt* expression level as an internal control for the assay. One representative result from a total of two repeats is shown. *C*, $CD4^+CD25^+$ T cells isolated from Aire-deficient mice (*a*, ■) dose-dependently suppressed [^{3}H]thymidine uptake by native T cells from wild-type mice cocultured in vitro with an efficiency nearly identical to that of $CD4^+CD25^+$ cells from control mice (○). $CD4^+CD25^-$ T cells (2.5×10^4) were mixed with $CD4^+CD25^+$ T cells in various ratios as indicated on the *x*-axis. $CD4^+CD25^-$ T cells (2.5×10^4) were isolated from Aire-deficient mice (*b*), and their suppressive function was examined as shown in *a*. One representative result from a total of two repeats is shown.

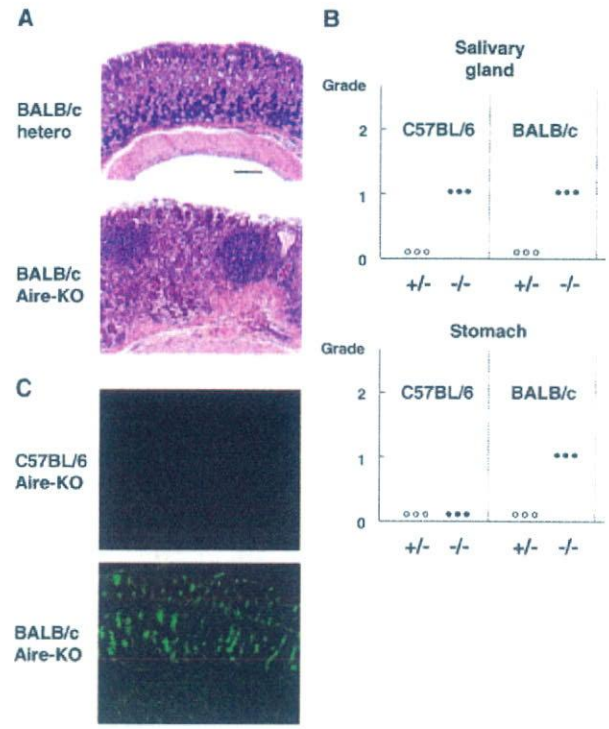

FIGURE 9. Strain-dependent target-organ specificity of the autoimmune disease caused by Aire deficiency. *A*, Aire-deficient BALB/c mice demonstrated lymphoid cell infiltration in the gastric mucosa (*bottom*). A scale bar corresponds to 100 μm in size (*top*; heterozygous Aire-deficient BALB/c mice). *B*, Aire-deficient BALB/c mice, but not Aire-deficient C57BL/6 mice, developed gastritis (*bottom*), whereas pathologic changes in the salivary glands were similarly observed in both strains (*top*). Histological changes in H&E-stained tissue sections were scored as shown in Fig. 2*B*. *C*, Aire-deficient BALB/c mice, but not Aire-deficient C57BL/6 mice, produced auto-Abs against gastric mucosa. Original magnification, ×100.

To gain further insight into how Aire contributes to the establishment of self-tolerance, we grafted control (Aire sufficient) and Aire-deficient embryonic thymus simultaneously into BALB/c *nude* mice. Inflammatory changes in the liver and pancreas of these animals were still present (Fig. 7*B*), supporting the hypothesis that impaired dominant control of autoreactive T cells by Tregs may not be the major defect caused by a thymic stroma lacking Aire; if impaired production of Tregs were the major defect caused by a thymic stroma lacking Aire, we assume that the defect should have been corrected by the grafted Aire-sufficient thymus. Therefore, it is reasonable to speculate that overproduction of autoreactive T cells plays an important role in the disease process triggered by Aire deficiency.

Strain-dependent target-organ specificity of the autoimmune disease caused by Aire deficiency

Although APECED is a monogenic disorder, it has been postulated that there may be additional factor(s) that determine the clinical features of the disease, such as the spectrum of affected organs (5, 6, 22). To test this hypothesis, we backcrossed our original strain of Aire-deficient mice to either the C57BL/6 ($H\text{-}2^b$) or BALB/c ($H\text{-}2^d$) strain for six generations. Both backcrossed strains showed autoimmune phenotypes similar to those from an original strain of Aire-deficient mice of mixed background (i.e., infiltration of many lymphoid cells in the salivary glands) (Fig. 9*B*, *top*). However, Aire-deficient BALB/c mice additionally demonstrated lymphoid cell infiltration in the gastric mucosa (Fig. 9, *A* and *B*, *bottom*), a feature that has been observed only rarely in the original Aire-deficient mice of mixed background (1 of 10) or Aire-deficient C57BL/6 mice (Fig. 9*B*, *bottom*). Consistent with these histological findings, serum harvested from Aire-deficient BALB/c mice (4 of 4) demonstrated strong auto-Abs against gastric mucosa (Fig. 9*C*), whereas this activity was observed in only one of four Aire-deficient C57BL/6 mice, and it was weak. Thus, the genetic background of the mice clearly influences the target-organ specificity of the disease caused by Aire deficiency.

Discussion

Using gene-targeted mice, we have investigated the mechanisms controlling the establishment and maintenance of self-tolerance by Aire. Both the numbers and suppressive function of $CD4^+CD25^+$ Tregs were not changed in Aire-deficient mice, when assessed in the adult mice. Using thymic chimeras, we also investigated possible defects in the production of any cell types (including

$CD4^+CD25^+$ Tregs) that are involved in the prevention of T cell-mediated organ-specific autoimmune diseases in the absence of Aire. When Aire-deficient and Aire-sufficient thymus were grafted simultaneously into *nude* mice, the development of inflammatory lesions was not completely inhibited. These results suggest that impaired production of Tregs may not be the major mechanism responsible for the breakdown of self-tolerance in Aire-deficient mice, and it is reasonable to speculate that the Aire-deficient thymus allows production of more pathogenic autoreactive T cells than could be controlled by the Tregs. However, it is important to emphasize that other aspects of Tregs, such as their repertoire formation, still remain unsolved; we cannot rule out the possibility that Aire may affect the Ag specificity of the Treg repertoire, because most of the analysis of the Tregs in the present study was quantitative rather than qualitative.

We have demonstrated that anti-α-fodrin autoimmunity developed in Aire-deficient mice despite the fact that the transcription of corresponding Ag (i.e., α-fodrin) in the thymic stroma was not down-regulated. Based on this finding, we suggest that Aire may regulate the processing and/or presentation of self-Ags by TECs, possibly through a coordinated action with BM-derived cells (see below), so that the maturing T cells can recognize the corresponding self-Ags in a form capable of efficiently triggering autoreactive T cells. It would be important to know whether our proposed model of Aire function in the establishment of self-tolerance is confined to ubiquitous self-Ags, such as α-fodrin, or applicable to tissue-specific Ags as well. In this regard, it is critical to investigate first whether autoimmunity develops bona fide against transcriptionally repressed tissue-specific Ags in the thymus in Aire-deficient mice. Definitively, identification of the substrate(s) for E3 ubiquitin ligase activity by AIRE should help to clarify the actual mechanisms of AIRE-dependent tolerance (10).

We have demonstrated that α-fodrin is one of the target Ags involved in the autoimmune-disease process caused by Aire deficiency. Because transfer of sera from affected mice did not result in the development of sialoadenitis or disruption of α-fodrin in the recipient mice (N. Ishimaru, R. Arakaki, and Y. Hayashi, unpublished observation), the disease process in Aire-deficient mice is most likely elicited by a cell-mediated immunity, as observed in the 3d-Tx-SS model (29, 30). Consistent with this hypothesis, splenocytes from Aire-deficient mice demonstrated proliferative responses in vitro when cultured with recombinant α-fodrin (Fig. 4).

Reduction of the intact form of α-fodrin in the affected lacrimal glands of some aged Aire-deficient mice (Fig. 6*B*) suggests that elicitation of autoreactivity against α-fodrin could be the primary pathogenetic process that leads to tissue destruction (27). In fact, adoptive transfer of α-fodrin-reactive T cells into ovariectomized B6 and SCID mice resulted in the development of autoimmune exocrinopathy quite similar to SS (30). However, based on the fact that α-fodrin is a ubiquitous protein and that the tissue destruction is confined to exocrine organs, it is reasonable to speculate that other undetermined tissue-specific target Ag(s) in exocrine organs might be additionally involved in the tissue destruction. Identification of precise target Ags involved in the disease process in Aire-deficient mice should help unravel the molecular mechanisms by which loss of Aire contributes to disease development.

We have demonstrated Aire-dependent disease development using allogeneic thymic chimeras; autoimmune disease commences in BALB/c *nude* recipients ($H\text{-}2^d$) of Aire-deficient, but not of wild-type, thymic transplants from mice of original mixed background ($H\text{-}2^{b/k} \times H\text{-}2^b$) (Fig. 7). The roles of TECs vs BM-derived cells in T cell repertoire selection in allogeneic thymic chimeras have been an issue of long-standing interest and debate. Given that *nude* mice reconstituted with an MHC-incompatible thymus generate effector T cells that are specific for the host and not for the thymic MHC (46), a novel mechanism may be responsible for the Aire-dependent negative selection; Aire expressed on TECs acts on BM-derived cells "in trans" as an important factor in organizing the "negative selection niche" in the thymus (47). This scenario is in good accordance with our results demonstrating the impaired tolerance to a ubiquitously expressed auto-Ag (i.e., α-fodrin) in Aire-deficient mice, because tolerance to ubiquitous self-proteins is mediated mainly by BM-derived cells in the thymus (48). Further study is required to test this intriguing hypothesis.

There is increasing evidence for the genetic complexity that underlies monogenic diseases (49, 50). In fact, the spectrum of the APECED phenotype is broad; the number of symptoms as well as the onset of each manifestation varies among affected patients. In our backcrossed mice, gastritis was observed predominantly in the BALB/c strain. In light of the fact that the individual HLA class II alleles modify the APECED phenotype (22), it is possible to speculate that MHC could be a candidate for the factor that determines this target-organ specificity. However, a genetic study with congenic strains has demonstrated that BALB/c ($H\text{-}2^d$), BALB.B ($H\text{-}2^b$), and BALB.K ($H\text{-}2^k$) were all susceptible to experimentally induced gastritis, whereas B10.D2 ($H\text{-}2^d$) were resistant, suggesting the predominant role of non-MHC gene(s) in determining susceptibility to autoimmune gastritis (51). Thus, MHC genes as well as non-MHC genes may together contribute to the complex phenotypes of APECED.

In conclusion, integration of detailed phenotypic analyses of Aire-deficient mice with current perspectives of thymus biology promises to illuminate many aspects of the molecular mechanisms responsible for the establishment and maintenance of self-tolerance. With the production of inbred strains of Aire-deficient mice, it may also be feasible to assess the impact of environmental factors that could influence the clinical features of APECED.

Acknowledgments

We thank Drs. W. van Ewijk and M. Itoi for the gift of ER-TR5 mAb. We thank Drs. T. Yamada, T. Yabuki, M. Kasai, and K. Iwabuchi for valuable suggestions. We also thank K. Awahayashi and F. Saito for technical assistance.

References

1. Kamradt, T., and N. A. Mitchison. 2001. Tolerance and autoimmunity. *N. Engl. J. Med. 344:655.*
2. Wanstrat, A., and E. Wakeland. 2001. The genetics of complex autoimmune diseases: non-MHC susceptibility genes. *Nat. Immunol. 2:802.*
3. Nagamine, K., P. Peterson, H. S. Scott, J. Kudoh, S. Minoshima, M. Heino, K. J. Krohn, M. D. Lalioti, P. E. Mullis, S. E. Antonarakis, et al. 1997. Positional cloning of the APECED gene. *Nat. Genet. 17:393.*
4. The Finnish-German APECED Consortium. 1997. An autoimmune disease, APECED, caused by mutations in a novel gene featuring two PHD-type zinc-finger domains. *Nat. Genet. 17:399.*
5. Björses, P., J. Aaltonen, N. Horelli-Kuitunen, M. L. Yaspo, and L. Peltonen. 1998. Gene defect behind APECED: a new clue to autoimmunity. *Hum. Mol. Genet. 7:1547.*
6. Pitkänen, J., and P. Peterson. 2003. Autoimmune regulator: from loss of function to autoimmunity. *Genes Immun. 4:12.*
7. Pitkänen, J., V. Doucas, T. Sternsdorf, T. Nakajima, S. Aratani, K. Jensen, H. Will, P. Vahamurto, J. Ollila, M. Vihinen, et al. 2000. The autoimmune regulator protein has transcriptional transactivating properties and interacts with the common coactivator CREB-binding protein. *J. Biol. Chem. 275:16802.*
8. Kumar, P. G., M. Laloraya, C. Y. Wang, Q. G. Ruan, A. Davoodi-Semiromi, K. J. Kao, and J. X. She. 2001. The autoimmune regulator (AIRE) is a DNA-binding protein. *J. Biol. Chem. 276:41357.*
9. Coscoy, L., and D. Ganem. 2003. PHD domains and E3 ubiquitin ligases: viruses make the connection. *Trends Cell Biol. 13:7.*
10. Uchida, D., S. Hatakeyama, A. Matsushima, H. Han, S. Ishido, H. Hotta, J. Kudoh, N. Shimizu, V. Doucas, K. I. Nakayama, et al. 2004. AIRE functions as an E3 ubiquitin ligase. *J. Exp. Med. 199:167.*
11. Hochstrasser, M. 1996. Ubiquitin-dependent protein degradation. *Annu. Rev. Genet. 30:405.*
12. Pickart, C. M. 2001. Mechanisms underlying ubiquitination. *Annu. Rev. Biochem. 70:503.*

13. Björses, P., M. Pelto-Huikko, J. Kaukonen, J. Aaltonen, L. Peltonen, and I. Ulmanen. 1999. Localization of the APECED protein in distinct nuclear structures. *Hum. Mol. Genet. 8:259.*
14. Heino, M., P. Peterson, J. Kudoh, K. Nagamine, A. Lagerstedt, V. Ovod, A. Ranki, I. Rantala, M. Nieminen, J. Tuukkanen, et al. 1999. Autoimmune regulator is expressed in the cells regulating immune tolerance in thymus medulla. *Biochem. Biophys. Res. Commun. 257:821.*
15. Kisielow, P., H. Bluthmann, U. D. Staerz, M. Steinmetz, and H. von Boehmer. 1988. Tolerance in T-cell-receptor transgenic mice involves deletion of nonmature $CD4^+8^+$ thymocytes. *Nature 333:742.*
16. Sakaguchi, S. 2004. Naturally arising $CD4^+$ regulatory T cells for immunologic self-tolerance and negative control of immune responses. *Annu. Rev. Immunol. 22:531.*
17. Shevach, E. M. 2002. $CD4^+CD25^+$ suppressor T cells: more questions than answers. *Nat. Rev. Immunol. 2:389.*
18. Kyewski, B., J. Derbinski, J. Gotter, and L. Klein. 2002. Promiscuous gene expression and central T-cell tolerance: more than meets the eye. *Trends Immunol. 23:364.*
19. Anderson, M. S., E. S. Venanzi, L. Klein, Z. Chen, S. Berzins, S. J. Turley, H. von Boehmer, R. Bronson, A. Dierich, C. Benoist, and D. Mathis. 2002. Projection of an immunological self-shadow within the thymus by the Aire protein. *Science 298:1395.*
20. Liston, A., S. Lesage, J. Wilson, L. Peltonen, and C. C. Goodnow. 2003. Aire regulates negative selection of organ-specific T cells. *Nat. Immunol. 4:350.*
21. Ramsey, C., O. Winqvist, L. Puhakka, M. Halonen, A. Moro, O. Kampe, P. Eskelin, M. Pelto-Huikko, and L. Peltonen. 2002. Aire deficient mice develop multiple features of APECED phenotype and show altered immune response. *Hum. Mol. Genet. 11:397.*
22. Halonen, M., P. Eskelin, A. G. Myhre, J. Perheentupa, E. S. Husebye, O. Kampe, F. Rorsman, L. Peltonen, I. Ulmanen, and J. Partanen. 2002. AIRE mutations and human leukocyte antigen genotypes as determinants of the autoimmune polyendocrinopathy-candidiasis-ectodermal dystrophy phenotype. *J. Clin. Endocrinol. Metab. 87:2568.*
23. Yagi, T., T. Tokunaga, Y. Furuta, S. Nada, M. Yoshida, T. Tsukada, Y. Saga, N. Takeda, Y. Ikawa, and S. Aizawa. 1993. A novel ES cell line, TT2, with high germline-differentiating potency. *Anal. Biochem. 214:70.*
24. Delporte, C., B. C. O'Connell, X. He, H. E. Lancaster, A. C. O'Connell, P. Agre, and B. J. Baum. 1997. Increased fluid secretion after adenoviral-mediated transfer of the aquaporin-1 cDNA to irradiated rat salivary glands. *Proc. Natl. Acad. Sci. USA 94:3268.*
25. Saegusa, K., N. Ishimaru, K. Yanagi, R. Arakaki, K. Ogawa, I. Saito, N. Katunuma, and Y. Hayashi. 2002. Cathepsin S inhibitor prevents autoantigen presentation and autoimmunity. *J. Clin. Invest. 110:361.*
26. Moon, R. T., and A. P. McMahon. 1990. Generation of diversity in nonerythroid spectrins. Multiple polypeptides are predicted by sequence analysis of cDNAs encompassing the coding region of human nonerythroid α-spectrin. *J. Biol. Chem. 265:4427.*
27. Haneji, N., T. Nakamura, K. Takio, K. Yanagi, H. Higashiyama, I. Saito, S. Noji, H. Sugino, and Y. Hayashi. 1997. Identification of α-fodrin as a candidate autoantigen in primary Sjögren's syndrome. *Science 276:604.*
28. Saegusa, K., N. Ishimaru, K. Yanagi, K. Mishima, R. Arakaki, T. Suda, I. Saito, and Y. Hayashi. 2002. Prevention and induction of autoimmune exocrinopathy is dependent on pathogenic autoantigen cleavage in murine Sjögren's syndrome. *J. Immunol. 169:1050.*
29. Arakaki, R., N. Ishimaru, I. Saito, M. Kobayashi, N. Yasui, T. Sumida, and Y. Hayashi. 2003. Development of autoimmune exocrinopathy resembling Sjögren's syndrome in adoptively transferred mice with autoreactive $CD4^+$ T cells. *Arthritis Rheum. 48:3603.*
30. Ishimaru, N., R. Arakaki, M. Watanabe, M. Kobayashi, K. Miyazaki, and Y. Hayashi. 2003. Development of autoimmune exocrinopathy resembling Sjögren's syndrome in estrogen-deficient mice of healthy background. *Am. J. Pathol. 163:1481.*
31. Ogawa, K., S. Nagahiro, R. Arakaki, N. Ishimaru, M. Kobayashi, and Y. Hayashi. 2003. Anti-α-fodrin autoantibodies in Moyamoya disease. *Stroke 34:e244.*
32. Gray, D. H., A. P. Chidgey, and R. L. Boyd. 2002. Analysis of thymic stromal cell populations using flow cytometry. *J. Immunol. Methods 260:15.*
33. Kajiura, F., S. Sun, T. Nomura, K. Izumi, T. Ueno, Y. Bando, N. Kuroda, H. Han, Y. Li, A. Matsushima, et al. 2004. NF-κB-inducing kinase establishes self-tolerance in a thymic stroma-dependent manner. *J. Immunol. 172:2067.*
34. Hori, S., T. Nomura, and S. Sakaguchi. 2003. Control of regulatory T cell development by the transcription factor FOXP3. *Science 299:1057.*
35. Matsumoto, M., Y.-X. Fu, H. Molina, G. Huang, J. Kim, D. A. Thomas, M. H. Nahm, and D. D. Chaplin. 1997. Distinct roles of lymphotoxin α and the type I tumor necrosis factor (TNF) receptor in the establishment of follicular dendritic cells from non-bone marrow-derived cells. *J. Exp. Med. 186:1997.*
36. Yamada, T., T. Mitani, K. Yorita, D. Uchida, A. Matsushima, K. Iwamasa, S. Fujita, and M. Matsumoto. 2000. Abnormal immune function of hemopoietic cells from alymphoplasia (*aly*) mice, a natural strain with mutant NF-κB-inducing kinase. *J. Immunol. 165:804.*
37. Itoh, M., T. Takahashi, N. Sakaguchi, Y. Kuniyasu, J. Shimizu, F. Otsuka, and S. Sakaguchi. 1999. Thymus and autoimmunity: production of $CD25^+CD4^+$ naturally anergic and suppressive T cells as a key function of the thymus in maintaining immunologic self-tolerance. *J. Immunol. 162:5317.*
38. Haneji, N., H. Hamano, K. Yanagi, and Y. Hayashi. 1994. A new animal model for primary Sjögren's syndrome in NFS/*sld* mutant mice. *J. Immunol. 153:2769.*
39. Nehls, M., B. Kyewski, M. Messerle, R. Waldschutz, K. Schuddekopf, A. J. Smith, and T. Boehm. 1996. Two genetically separable steps in the differentiation of thymic epithelium. *Science 272:886.*
40. Farr, A. G., and S. K. Anderson. 1985. Epithelial heterogeneity in the murine thymus: fucose-specific lectins bind medullary epithelial cells. *J. Immunol. 134:2971.*
41. Van Vliet, E., M. Melis, and W. van Ewijk. 1984. Monoclonal antibodies to stromal cell types of the mouse thymus. *Eur. J. Immunol. 14:524.*
42. Fontenot, J. D., M. A. Gavin, and A. Y. Rudensky. 2003. Foxp3 programs the development and function of $CD4^+CD25^+$ regulatory T cells. *Nat. Immunol. 4:330.*
43. Khattri, R., T. Cox, S. A. Yasayko, and F. Ramsdell. 2003. An essential role for Scurfin in $CD4^+CD25^+$ T regulatory cells. *Nat. Immunol. 4:337.*
44. Viglietta, V., C. Baecher-Allan, H. L. Weiner, and D. A. Hafler. 2004. Loss of functional suppression by $CD4^+CD25^+$ regulatory T cells in patients with multiple sclerosis. *J. Exp. Med. 199:971.*
45. Kriegel, M. A., T. Lohmann, C. Gabler, N. Blank, J. R. Kalden, and H. M. Lorenz. 2004. Defective suppressor function of human $CD4^+CD25^+$ regulatory T cells in autoimmune polyglandular syndrome type II. *J. Exp. Med. 199:1285.*
46. Zinkernagel, R. M., and A. Althage. 1999. On the role of thymic epithelium vs. bone marrow-derived cells in repertoire selection of T cells. *Proc. Natl. Acad. Sci. USA 96:8092.*
47. Kyewski, B., and J. Derbinski. 2004. Self-representation in the thymus: an extended view. *Nat. Rev. Immunol. 4:688.*
48. Sprent, J., and C. D. Surh. 2003. Knowing one's self: central tolerance revisited. *Nat. Immunol. 4:303.*
49. Estivill, X. 1996. Complexity in a monogenic disease. *Nat. Genet. 12:348.*
50. Weatherall, D. J. 2000. Single gene disorders or complex traits: lessons from the thalassaemias and other monogenic diseases. *Br. Med. J. 321:1117.*
51. Sakaguchi, S., and N. Sakaguchi. 2000. Role of genetic factors in organ-specific autoimmune diseases induced by manipulating the thymus or T cells, and not self-antigens. *Rev. Immunogenet. 2:147.*

Exp. Anim. 53(2), 171–173, 2004

—Note—

Differences in Responsiveness of Mouse Strain against p-Benzoquinone as Assessed by Non-Radioisotopic Murine Local Lymph Node Assay

Masahiro TAKEYOSHI, Shuji NODA, and Kanji YAMASAKI

Hita Laboratory, Chemicals Evaluation and Research Institute, Japan, 3–822, Ishii-machi, Hita-shi, Oita 877-0061, Japan

Abstract: *The non-radioisotopic modification of murine local lymph node assay (LLNA) by using 5-bromo-2'-deoxyuridine (BrdU) was conducted to investigate the strain-related difference of the responsiveness of mice to* p*-benzoquinone (PBQ) with BALB/cAnN, CBA/JN and CD-1 mouse strains. Strain and dose related differences were analyzed by two-way analysis of variance (two-way ANOVA). CBA/JN was considered to be the highest responsive strain to PBQ, and interaction was detected between CD-1 and each of the other inbred strains. These results support the recommendation in the OECD test guideline 429 and the skin sensitization test guideline of US-EPA with regard to the selection of mouse strain for LLNA.*

Key words: *local lymph node assay, responsiveness,* p*-benzoquinone*

Contact dermatitis caused by chemicals is a serious health problem, and a prediction of the skin sensitizing potential of chemicals is necessary to secure safe handling of chemicals. The guinea pig maximization test and the Buehler test have been widely used for predicting the skin sensitizing potentials of chemicals for regulatory purposes for a long time [1, 6]. Recently the murine local lymph node assay (LLNA) has been recognized as a new stand-alone sensitization test which can be used for regulatory purposes [3–5], and it is based upon consideration of the induced proliferative responses in lymph nodes draining the site of topical exposure to the test chemical. In the standard LLNA, cell proliferation is measured using the incorporation of radiolabeled thymidine or uridine into draining lymph node cells, and this requires specific facilities and handling conditions. We previously developed a non-radioisotopic alternative method for the LLNA which uses 5-bromo-2'-deoxyuridine (BrdU) incorporation in place of radioisotopes [9, 10]. The responsiveness of mouse strains against antigen is known to vary with their H-2 haplotypes. We report here the difference of responsiveness of three mouse strains in the modified murine local lymph node assay against *p*-benzoquinone, a known potent contact allergen to human.

p-Bebzoquinone (BZQ, Lot No. 012D2294, Kanto Chemical Co., Tokyo, Japan) was dissolved in acetone:olive oil (AOO; 4:1). 5-Bromo-2'-deoxyuridine (BrdU, Nacalai Tesque, Kyoto, Japan) was dissolved in

(Received 22 September 2003 / Accepted 25 December 2003)

Address corresponding: M. Takeyoshi, Hita Laboratory, Chemicals Evaluation and Research Institute, Japan, 3–822, Ishii-machi, Hita-shi, Oita 877-0061, Japan

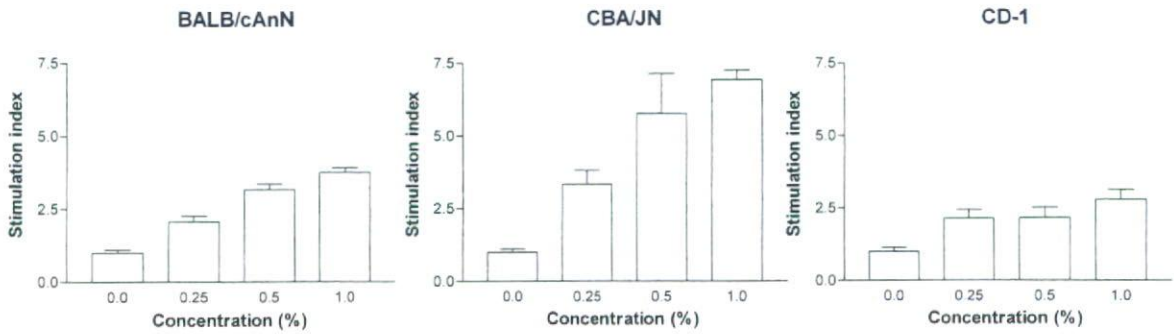

Fig. 1. Dose responses in the modified local lymph node assay with *p*-benzoquinone.
*Data are represented as the mean ± standard error.

physiological saline at a concentration of 10 mg/ml. Female CBA/JN, BALB/cAnN and CD-1 mice were obtained from Charles River Japan Ltd. (Kanagawa, Japan). Mice were housed in animal rooms maintained at a temperature of 23 ± 2°C and relative humidity of 55 ± 15%. The rooms were ventilated at a frequency of 10 to 15 cycles/h, and lighted artificially for 12 h daily.

Mice were randomly allocated to 4 groups (4 mice/group) per each strain of mouse. A 25 µl volume of PBQ in AOO was applied to the dorsum of both ears of the mice daily for three consecutive days. A single intraperitoneal injection (5 mg/mouse/injection) of BrdU was made on day 4. On day 5, auricular lymph nodes were removed, weighed, and stored at –20°C until analysis by an ELISA to measure BrdU incorporation.

BrdU incorporation into the lymph node cells was determined using a commercial cell proliferation assay kit (Boehringer Mannheim Corp., Indianapolis, IN, USA, Cat. No. 1647229). Lymph nodes were crushed, and after passage through a #70 nylon mesh, the cells were suspended in 15 ml of physiological saline. The cell suspension (100 µl) was added to the wells of a flat-bottom microplate (Coster 3595, Corning Inc., NY, USA) in quadruplicate. After centrifugation (3000 × g, 10 min), the supernatants were removed, 200 µl of Fix-Denat solution was added to each well, and then the plate was allowed to stand for 30 min at room temperature. After removing the Fix-Denat solution, diluted anti-BrdU antibody solution (100 µl, Boehringer Mannheim Corp.) was added to each well, and after rinsing 3 times with washing buffer (phosphate-buffered saline), 100 µl of substrate solution containing tetramethylbenzidine (TMB) was added and allowed to react for 15 min at room temperature. Absorbance at 370 nm was determined as the BrdU labeling index with a microplate reader (SpectraMAX™, Molecular Devices Inc., Sunnyvale, CA, USA) at a reference wavelength of 492 nm. Means and standard errors for the labeling indices were calculated for each treatment group, and the stimulation index (SI) was calculated by dividing the labeling indices in each test group by that in the concurrent vehicle control group. Then, two-way analysis of variance (Two-way ANOVA) was performed with regard to dose and strain as factors.

Dose responses against PBQ for each mouse strain are shown in Fig. 1. The SI values for 0.25%, 0.5% and 1% PBQ were 3.4, 5.8 and 6.9 in CBA/JN, 2.1, 3.2, and 3.8 in BALB/cAnN, and 2.1, 2.2 and 2.8 in CD-1, respectively. The SI values increased in a dose dependent manner in all mouse strains. Positive responses (SI>3) were noted ≥0.25% in CBA/JN, ≥0.5% in BALB/cAnN and >1.0% in CD-1. As the results of two-way ANOVA, CBA/JN showed the highest responsiveness to PBQ, and interaction was noted between CD-1 and each of the other inbred strains (Table 1). Consequently, CBA/JN was considered to be the highest responder strain to PBQ, and CD-1 is not a preferable strain for LLNA. In the OECD and US-EPA guidelines [2, 8], and the ICCVAM validation report for LLNA [7], CBA/Ca or CBA/J mouse are recommended for selection of animal species. In this study, the CBA/JN mouse showed the highest responsiveness to PBQ among three mouse strains tested. Our result supports the animal selection described in the test guidelines and the review article mentioned above.

Table 1. Probabilities detected in two-way analysis of variance (two-way ANOVA)

Source of Variation	CBA/JN vs. BALB/cAnN		CBA/JN vs. CD-1		BALB/cAnN vs. CD-1	
Interaction	0.2209	ns	0.0076	**	0.0125	*
Strain	0.0385	*	0.0001	***	<0.0001	***
Dose	<0.0001	***	<0.0001	***	<0.0001	***

Asterisks indicate significance levels (*: P<0.05, **: P<0.01, ***: P<0.001). ns: not significant.

Acknowledgments

We wish to thank Ms. Nobuko Mitoma, Ms. Naoko Kuga and Ms. Satoko Sakamoto for their skillful technical assistance.

References

1. Buehler, E.V. 1995. Methods in Immunotoxicology, 2, 343–356, A John Wiley & Sons, Inc. New York.
2. Environmental Protection Agency (EPA). 2003. Health Effects Test Guidelines OPPTS 870.2600.
3. Gerberick, G.F., Ryan, C.A., Kimber, I., Dearman, R.J., Lea, L.J., and Basketter, D.A. 2000. *Am. J. Contact Derm.* 11: 3–18.
4. Kimber, I., Dearman, R.J., Scholes, E.W., and Basketter, D.A.1994. *Toxicology* 93: 13–31.
5. Kimber, I., Hilton, J., Dearman, R.J., Gerberick, G.F., Ryan, C.A., Basketter, D.A., Scholes, E.W., Ladics, G.S., Loveless, S.E., House, R.V. and Guy, A. 1995. *Toxicology.* 103: 63–73.
6. Magnusson, B. and Kligman, A.M. 1969. *J. Invest. Dermatol.* 52: 268–276.
7. National Institute of Environmental Health Sciences (NIEHS). 1999. NIH Publication No: 99-4494, Research Triangle Park, N.C.
8. Organization for Economic Corporation and Development (OECD). 2002. Health effect test guideline-429 (Adopted: 24th April 2002).
9. Takeyoshi, M., Yamasaki, K., Yakabe, Y., Takatsuki, M., and Kimber, I. 2001. *Toxicology Letters.* 119: 203–208.
10. Takeyoshi, M., Sawaki1, M., Yamasaki, K., and Kimber, I. 2003. *Toxicology* 191: 259–263.

JOURNAL OF APPLIED TOXICOLOGY
J. Appl. Toxicol. **24**, 77–81 (2004)
Published online in Wiley InterScience (www.interscience.wiley.com). **DOI:** 10.1002/jat.951

Assessment of the Skin Sensitization Potency of Eugenol and its Dimers using a Non-radioisotopic Modification of the Local Lymph Node Assay

Masahiro Takeyoshi,[1]* Shuji Noda,[1] Shunsuke Yamazaki,[2] Hiroshi Kakishima,[2] Kanji Yamasaki[1] and Ian Kimber[3]

[1] Chemicals Assessment Center, Chemicals Evaluation and Research Institute, 3-822, Ishii-machi, Hita-shi, Oita 8770061, Japan
[2] Cosmetic Laboratory, Kanebo Ltd., 5-3-28, Kotobuki-cho, Odawara, Kanagawa 2500002, Japan
[3] Syngenta Central Toxicology Laboratory, Alderley Park, Macclesfield, Cheshire, SK10 4TJ, UK

Key words: eugenol, local lymph node assay, non-radioisotopic, potency, sensitization.

Allergic contact dermatitis is a serious health problem. There is a need to identify and characterize skin sensitization hazards, particularly with respect to relative potency, so that accurate risk assessments can be developed. For these purposes the murine local lymph node assay (LLNA) was developed. Here, we have investigated further a modification of this assay, non-radioisotopic LLNA, which in place of tritiated thymidine to measure lymph node cell proliferation employs incorporation of 5-bromo-2′-deoxyuridine. Using this method we have examined the skin sensitizing activity of eugenol, a known human contact allergen, and its dimers 2,2′-dihydroxyl-3,3′-dimethoxy-5,5′-diallyl-biphenyl (DHEA) and 4,5′-diallyl-2′-hydroxy-2,3′-dimethoxy phenyl ether (DHEB). Activity in the guinea pig maximization test (GPMT) also measured. On the basis of GPMT assays, eugenol was classified as a mild skin sensitizer, DHEA as a weak skin sensitizer and DHEB as an extreme skin sensitizer. In the non-radioisotopic LLNA all chemicals were found to give positive responses insofar as each was able to provoke a stimulation index (SI) of ≥3 at one or more test concentrations. The relative skin sensitizing potency of these chemicals was evaluated in the non-radioisotopic LLNA by derivation of an EC_3 value (the concentration of chemical required to provoke an SI of 3). The EC_3 values calculated were 25.1% for eugenol, >30% for DHEA and 2.3% for DHEB. Collectively these data suggest that assessments of relative potency deriving from non-radioisotopic LLNA responses correlate well with evaluations based on GPMT results. These investigations provide support for the proposal that the non-radioisotopic LLNA may serve as an effective alternative to the GPMT where there is a need to avoid the use of radioisotopes. Copyright © 2004 John Wiley & Sons, Ltd.

INTRODUCTION

Allergic contact dermatitis is an important occupational and environmental health problem and there is a continuing need to identify accurately potential skin sensitization hazards and to assess effectively the likely risks to human health. Various methods have been developed for the assessment of skin sensitization potential, including those using guinea pigs, such as the guinea pig maximization test (GPMT) (Magnusson & Kligman, 1969) and Buehler's occluded patch test (Buehler, 1995), and more recently the murine local lymph node assay (LLNA) (Kimber *et al.*, 1994, 1995; Loveless *et al.*, 1996; Gerberick *et al.*, 2000). In the GPMT and the Buehler's occluded patch test the skin sensitizing potential is determined as a function of challenge-induced reactions in previously sensitized guinea pigs, whereas the LLNA is based upon consideration of induced proliferative responses in lymph nodes draining the site of topical exposure to the test chemical. In addition to hazard assessment, attention has focused more recently on evaluation of the relative skin sensitization potency as a first step in the risk assessment process. The view is that the LLNA is particularly suited to this application, not least because it is known that the vigour of lymphocyte proliferative responses induced in skin-draining lymph nodes correlates closely with the extent to which sensitization will develop.

In the standard LLNA a chemical is classified as a skin sensitizer if at one or more test concentrations it is able to induce a threefold or greater increase in lymph node cell proliferation, i.e. a stimulation index (SI) of ≥3. For the purposes of evaluating relative potency, an EC_3 value is derived mathematically from consideration of LLNA dose responses, EC_3 being the amount of contact allergen necessary to induce an SI of 3. Although the LLNA has proved to be a robust and reliable method for evaluation of skin sensitization hazards and risks, one feature that has

* Correspondence to: M. Takeyoshi, Chemicals Assessment Center, Chemicals Evaluation and Research Institute, 3-822, Ishii-machi, Hita-shi, Oita 8770061, Japan.
E-mail: takeyoshi-masahiro@ceri.jp

Copyright © 2004 John Wiley & Sons, Ltd.

Received 4 July 2003
Revised 26 August 2003
Accepted 3 September 2003

sometimes limited its application is the need for a radioisotope. In the standard LLNA, lymph node cell proliferation is measured on the basis of incorporation by cells of [^{3}H]thymidine (^{3}HTdR).

We have previously explored the utility of a modified version of the assay in which, in place of radiolabelled thymidine, cell turnover is measured using the incorporation of 5-bromo-2′-deoxyuridine (BrdU) (Takeyoshi *et al.*, 2001). Here we describe investigations to explore further the value of this non-radioisotopic LLNA for the purposes of hazard identification and the determination of relative potency. To this end, responses to three chemicals have been measured: eugenol, a known contact allergen, and its dimers 2,2′-dihydroxyl-3,3′-dimethoxy-5,5′-diallyl-biphenyl (DHEA) and 4,5′-diallyl-2′-hydroxy-2,3′-dimethoxy phenyl ether (DHEB). For comparative purposes the activity of each of these three chemicals was also measured using the GPMT.

EXPERIMENTAL

Chemicals and reagents

Eugenol (lot no. EG0704; >95%), 2,2′-dihydroxyl-3,3′-dimethoxy 5,5′-diallyl-biphenyl (DHEA: lot no. DHEA0704; >95%) and 4,5′-diallyl-2′-hydroxy-2,3′-dimethoxy phenyl ether (DHEB: lot no. DHEB0704; >95%) were kindly donated by Kanebo Cosmetics Company (Odawara, Kanagawa, Japan) (Fig. 1). Eugenol and its dimers were dissolved in olive oil for the GPMT or in acetone–olive oil (AOO, 4 : 1) for the non-RI LLNA. 5-Bromo-2′-deoxyuridine (BrdU; Nacalai Tesque, Kyoto, Japan) was dissolved in physiological saline at a concentration of 10 mg ml^{-1}.

Animals

Female Hartley guinea pigs and CBA/JN strain mice were obtained from SLC Japan Ltd (Shizuoka, Japan) and Charles River Japan Ltd (Kanagawa, Japan), respectively. The animals were housed in animal rooms maintained at a temperature of 22 ± 3 °C and at a relative humidity of 55 ± 15%. The rooms were ventilated at a frequency of 10–15 cycles per hour and lighted artificially for 12 h daily. Animals were allowed free access to a laboratory diet (RC-4 for guinea pigs and MF for mice; Oriental Yeast Co., Tokyo, Japan) and tap water.

Experimental designs

Guinea pig maximization test. Guinea pigs were allocated randomly to three groups (10 animals per group). The test was conducted according to a method described previously (Magnusson & Kligman, 1969). Guinea pigs received a series of intradermal injections of eugenol or its dimers in the shoulder region to induce sensitization. After 6–8 days, sensitization was boosted by a 48-h occluded patch of the same compound placed over the injection sites. Fourteen days later, the animals were challenged on a shaved flank by a 24-h occluded patch containing the same compound. All induction and challenge concentrations were set at 5% (maximum non-irritant concentration) in olive oil for all compounds in view of preliminary dose-finding tests. All compounds elicited an apparent irritation at 10% in preliminary tests for intradermal injection and topical application, so we decided on induction and challenge concentrations of 5% for all compounds in order to compare the sensitization potency of these three compounds. Chemicals were classified by the sensitization rate for each chemical (0–8%, weak; 9–28%, mild; 29–64%, moderate; 65–80%, strong; 81–100%, extreme) according to the criteria given by Magnusson and Kligman (1969).

Non-radioisotopic LLNA. Mice were allocated randomly to 11 groups (four animals per group). A 25-μl volume of test chemicals at concentrations of 1%, 6%, 15% or 30% for eugenol, 1%, 6% or 30% for DEHA and 1%, 6% or 20% for DEHB was applied to the dorsum of both ears of the mice daily for three consecutive days. The concentration ranges of each test chemical were decided according to the sensitization potencies classified by the results of GPMT. A single intraperitoneal injection (5 mg per mouse per injection) of BrdU was then given on day 4. On day 5, the draining auricular lymph nodes were

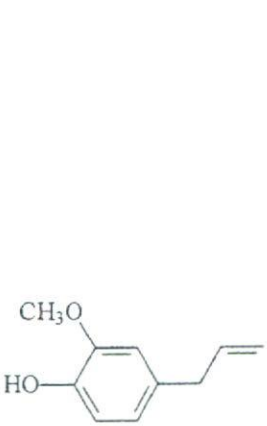

Eugenol

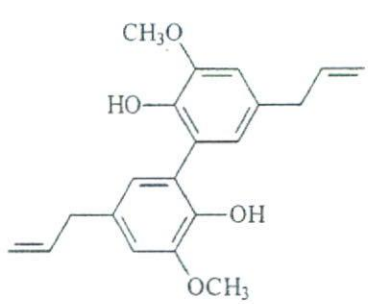

2,2′-dihydroxyl-3,3′-dimethoxy-5,5′-diallyl-biphenyl (DHEA)
- Eugenol dimer 1 -

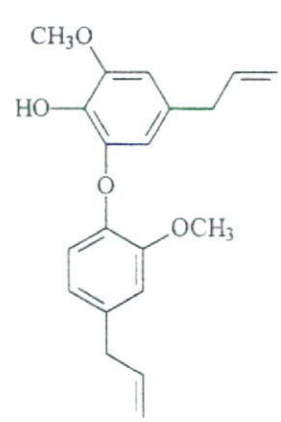

4,5′-diallyl-2′-hydroxy-2,3′-dimethoxy phenyl ether (DHEB)
- Eugenol dimer 2 -

Figure 1. Chemical structures of eugenol and its dimers used in this study.

Copyright © 2004 John Wiley & Sons, Ltd.

removed, weighed and stored at −20 °C until analysis using an enzyme-linked immunosorbent assay (ELISA) to measure BrdU incorporation. The incorporation of BrdU into lymph node cells was determined using a commercial cell proliferation assay kit (Boehringer Mannheim Corp., Indianapolis, IN, USA; Cat. no. 1647229). The lymph nodes were crushed, passed through a no. 70 nylon mesh and the lymph node cells were suspended in 15 ml of physiological saline individually. The cell suspension (100 µl) was added to the wells of a flat-bottom microplate (Coster 3595; Corning Inc., NY, USA) in triplicate. After centrifugation (3000 *g*, 10 min), the supernatants were removed. A 200-µl volume of Fix-Denat solution was added to each well and then the plate was allowed to stand for 30 min at room temperature. After removing the Fix-Denat solution, diluted anti-BrdU antibody solution (100 µl, Boehringer Mannheim Corp.) was added to each well and, after rinsing three times with washing buffer (phosphate-buffered saline), 100 µl of substrate solution containing tetramethylbenzidine (TMB) was added and allowed to react for 15 min at room temperature. Absorbance at 370 nm was determined with a microplate reader (SpectraMAX™, Molecular Devices Inc., Sunnyvale, CA, USA) at a reference wavelength of 492 nm. The absorbance was defined as the BrdU labelling index.

Statistical analysis

Means and standard errors were calculated for the labelling index obtained by ELISA for each treatment group. The SI values relative to the AOO-treated control value were then calculated. Data were analysed simultaneously using the Bartlett test for homogeneity of variance. If the variances were homogeneous at a level of 5% significance, a one-way analysis of variance (one way-ANOVA) was performed. If the one-way ANOVA produced a significant difference, the differences between the control group and each of the experimental groups were analysed using the Dunnett test. If the variances were not homogeneous, the Kruskal–Wallis test was employed. If this test produced a significant difference, the difference between the control group and each of the experimental groups was analysed using the non-parametric Dunnett test (Bruning & Kintz, 1997).

Measurement of EC_3 values

The estimated concentration of a chemical required to induce an SI of 3 relative to vehicle-treated controls (EC_3 value) was derived by linear interpolation as described previously (Basketter *et al.*, 2000). The EC_3 value was calculated by interpolating between two points on the SI axis, one immediately above and one immediately below the SI value of 3. The vehicle-treated control value (SI = 1) cannot be used for the latter. Where the data points lying immediately above and below the SI value of 3 have the coordinates (a, b) and (c, d), respectively, then the EC_3 value may be calculated using the following equation:

$$EC_3 = c + [(3 - d)/(b - d)](a - c)$$

RESULTS

Guinea pig maximization test

In the GPMT for eugenol and its dimers, the sensitization response rates were as follows: eugenol, 20%; DHEA, 0%; DHEB, 100%. According to convention (Magnusson & Kligman, 1969) therefore, eugenol was classified as a mild skin sensitizer; DHEA as a weak skin sensitizer and DHEB as an extreme skin sensitizer (Table 1).

Non-radioisotopic LLNA

At application concentrations of 15% or greater, exposure of mice to eugenol caused a significant increase in draining lymph node weight compared with concurrent vehicle-treated controls (see Table 2). A positive response with respect to lymph node cell proliferation was obtained with 30% eugenol (SI = 3.3). Significant increases in the incorporation of BrdU were observed following treatment with both 15% and 30% eugenol, but at the lower concentration this did not translate into a positive response with respect to the stimulation index (SI = 2.3). The DHEA dimer failed to induce a positive response in the nonradioisotopic LLNA at any concentration tested, although at the highest concentration (30%) there was a significant increase in BrdU incorporation compared with vehicle-treated controls. The highest concentrations of DHEA were without effect on draining lymph node weight, although at the lowest concentration of this dimer tested there was a significant increase. Finally, the second dimer (DHEB) provoked clear positive responses in the non-radioisotopic LLNA. Treatment with 6% DHEB resulted in SI = 5.0 and treatment with 20% DHEB produced SI = 7.2. At both of these test concentrations there was also a statistically significant increase in the incorporation by lymph node cells of BrdU compared with controls. At all concentrations of DHEB examined there were significant increases in lymph node weight.

The EC_3 values for eugenol and DHEB were calculated using a standard method and were found to be 25.1% and 2.3%, respectively. Such an approach was not possible with DHEA because at no test concentration was a positive response elicited in the non-radioisotopic LLNA with respect to an SI of ≥3. An EC_3 value for DHEA has therefore been estimated, for the purposes of comparison, by linear extrapolation of the dose–response curve. Although this is somewhat unconventional, it is considered acceptable in

Table 1—Results of the guinea pig maximization test for eugenol and its dimers

Chemical name	Sensitization rate (%)	Classification[a]
Eugenol	20	Mild
2,2′-Dihydroxyl-3,3′-dimethoxy-5,5′-diallyl-biphenyl (DHEA)	0	Weak
4,5′-Diallyl-2′-hydroxy-2,3′-dimethoxy phenyl ether (DHEB)	100	Extreme

[a] Classified according to the criteria of Magnusson and Kligman (1969).

Copyright © 2004 John Wiley & Sons, Ltd.